AMAS Course on Mechanics of Advanced Materials
MAM'2001 – (pp.235–306) – Warsaw, October 8-12, 2001.

Application of powder diffraction methods to the analysis of the atomic structure of nanocrystals: theory and experiment

B. PAŁOSZ

High Pressure Research Center UNIPRESS,
Sokołowska 29/37, 01-142 Warsaw, Poland
e-mail: palosz@unipress.waw.pl

I. The capabilities and limitations of conventional powder diffractometry. The concept of *alp*. The applicability of standard methods of elaboration of powder diffraction data of nanosize crystallites is analysed. Based on theoretical calculations of powder diffraction data it is shown, that the assumption of the infinite crystal lattice for small particles is not justified, leads to significant changes of the diffraction patterns, and may lead to erroneous interpretation of the experimental results. An alternate evaluation of diffraction data of nanoparticles, based on the so-called "apparent lattice parameter", *alp*, is proposed. Based on this new methodology it is shown that real nano-crystals constitute a complex, more than a one-uniform-phase structure.

II. High-pressure studies of nanocrystalline materials. High-pressure X-ray diffraction techniques were applied to study the structural properties of nanocrystalline ceramic powders of SiC and GaN. Limitations and capabilities of this investigative tool due to the nature of the sample itself (non-uniform atomic structure) and the experimental technique (which gives information averaged over the entire volume of the sample) are discussed. We show that due to their complex structure (a two-phase, core/surface shell system) no unique value of compressibility can satisfactorily describe the behavior of such materials under pressure. We offer a tentative interpretation of the distribution of *macro*- and *micro*-strains in nanoparticles of different grain size. For the interpretation of high-pressure diffraction data we apply a concept of the *apparent lattice parameter* and its dependence on the diffraction vector Q. The *alp*-Q plots are characteristic for nanopowders with different grain sizes and depend on pressure. This work gives an experimental evidence of the existence of the core/shell model of nanocrystalline SiC and GaN.

Key words: *nanocrystals, high pressure, surface structure, diffraction.*

I. The capabilities and limitations of conventional powder diffractometry. The concept of *alp*.

1. Introduction

The atomic structure of materials is determined by the sum of long-range forces irrespective of the size of the object. The actual structure of a particle is, however,

dependent on its size. This dependence can be ignored for large particles – crystallites, but it must be taken into account when the characteristic dimension of an assemble of atoms is comparable to the effective radius of the long-range interactions. This applies in particular to nanocrystals which can be as small as a few nanometers only.

Nanocrystals belong to a general class of polycrystalline materials and are distinguished as a separate class due to their small size and related unique properties. The occurrence of nanoparticles with a well-defined crystallographic structure can be predicted directly from the concept of formation and stability of atomic clusters (AC) [1-3]. Based on the general considerations of mutual interactions, an array of randomly arranged atoms tends, under certain conditions, to transform to well ordered aggregates – atomic clusters. This process is observed during crystallization of solids from an amorphous condensed matrix (e.g., a melt) or the gas phase. The atomic clusters existing under various environment conditions have different surface energies: the energy of an isolated particle (in vacuum) is larger than that "embedded" in a matrix material. Based on direct Ultra-High Voltage Electron Microscope (HVEM) observations of formation of crystalline particles of different materials, the so-called "magic sizes", d_M, were measured [1, 2]. Above the "magic size" (critical size), which is the material property, the atomic clusters show a strong tendency to long-range ordering of the constituent atoms. The "magic size" values were determined for a number of metals and ceramics directly from the observations of amorphization and/or recrystallization occurring under HVEM conditions. The actual value of d_M is a function of the bonding mode, binding force, and depends on the surrounding media [1, 2]. Different properties (and behavior) of surface and interior atoms can be deduced and characterized based on the concept of atomic clusters.

Obvious differences between binding energies of the atoms arranged in molecules, small clusters, or bulk solids exist. The force behind ordering of atoms in a periodic lattice is the presence of a many-body-potential (*mbp*). Each specific atomic structure is associated with an *mbp*, which is necessary for the creation of hybrid orbitals between the individual constituent atoms. The hybrid orbitals, in turn, are able to

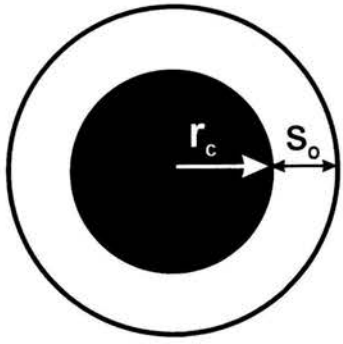

FIGURE 1. Schematic diagram of an atomic cluster. r_c is the radius of the grain core, s_0 is the thickness of the buffer zone.

form periodic hybrid orbitals and to arrange the individual atoms into a three dimensional lattice. There is a minimum number of atoms required for the formation of "complete" hybrid orbitals. In a finite object there is always a discontinuity of the atomic structure at the surface, what leads to the presence of a surface energy. The hybrid orbitals at the surface of an isolated particle are different than those in the bulk, therefore the atomic structure of the surface is different than that in the grain core. In other words, the *mbp* has a different effect on the relative positions of the surface and interior atoms, so the atomic structure of the surface of a solid is different than that of the corresponding relaxed crystal lattice. It is demonstrated schematically in Fig. 1 for an atomic cluster with atoms having complete hybrid orbitals and a perfect crystal lattice forming the particle center ($r < r_c$) and the outer buffer zone of thickness s_0.

The "magic size" d_M of an isolated particle can be expressed as:

$$d_M = 2\Lambda = 2(r_c + r_c^*) + a = (4P + 1)a, \tag{1.1}$$

where Λ is the effective radius of long-range forces (LRF), r_c is the minimum radius of a sphere where the hybrid orbital can be established, r_c^* is the thickness of the "buffer zone" surrounding the particle core, $r_c^* \approx r_c$, $P = r_c/a$, and a is the atom diameter.

A presence of the "buffer zone" with thickness r_c^* (here: s_0 in Fig. 1), is necessary to relax the effect of the surface on the formation of hybrid orbitals in the interior of the particle. One can say that the "buffer zone" constitutes the nanoparticle surface shell. The positions of the atoms in the shell are determined by the "parent structure" (i.e. that of the interior of the grain, the core) and by the atoms surrounding the particle. It was estimated that the thickness of the "buffer zone" of a particle embedded in a disordered medium of the parent material (e.g., a crystallite embedded in an amorphous matrix) is two times thinner than that of an isolated particle [2].

Based on HVEM observations it was found that the critical size of an atomic cluster required for periodic ordering decreases with an increase of the degree of covalency and with a decrease in the coordination number. Consequently, assuming that the thickness of the layer is equal to that of the "buffer zone", it is thinner in particles with stronger bonds between the atoms. Using d_M values for isolated atomic clusters (we will call them nanoparticles) with a diamond-type structure, the expected surface layer thickness is between 1 and 2.5 nm (for metals it can be as large as 10 nm). The same particles embedded in a disordered matrix may be expected to have the surface layer thinner by a factor of 2, i.e. to have the thickness between 0.5 nm in diamond-type structures and 5 nm in metals. No experimentally determined specific thickness of the surface shell of nanocrystals, or the "degree of strain" at the surface layer has been reported in the literature yet.

The effect of *mbp* on ordering of the outer atomic layers may be expected to decrease monotonically from the interior towards the surface of the particle. It is obvious that the atomic structure of the inner boundary of the surface layer must be the same as that of the grain core. The deviation of this structure from the matrix should increase towards the most external atomic layer. A simple definition of the "surface layer thickness" is that it is equal to that of the "buffer zone". However, we

are not aware of any experimental methods which could be used to measure the as-defined thickness of the surface layer of nanoparticles. To *discern between the surface and interior phases of a grain,* their physical and/or structural properties must be sufficiently different to be experimentally measurable. In this work *we discuss this problem with regard to the capabilities of the powder diffraction techniques.*

The properties of nanocrystalline materials are critically dependent on the atomic structure of the constituent grains. A size-dependent atomic structure of nanoparticles may lead to unique properties (like unusual hardness or superplasticity, different melting temperature or luminescence spectra, etc.) of nanomaterials relative to conventional polycrystals of the same substance, [4-8]. However, different than for micro-sized materials, the properties of nanoparticles pose a technological challenge in the production of large-volume, dense nanomaterials. For instance, due to an enhanced surface and/or bulk diffusion during the sintering process a fast coarsening of the grains occurs what leads to irreversible loss of the unique properties conditioned by the small size of individual grains. The surface of individual crystallites apparently plays an important role in this and other phenomena.

In conventional polycrystalline materials with micrometer size grains the surface atoms constitute only a small fraction of total number of atoms and their effect on the overall properties of the material can be ignored. The situation is different in small, nanosize particles where, due to their size, a considerable fraction of the atoms forms the surface of the grain. As showed in Fig. 2, an abrupt termination of a perfect crystal lattice (Fig. 2a) leaves the outmost atoms without some of their neighbors (Fig. 2b) what leads either to a reconstruction of the surface or to generation of strains through changes of the length of the interatomic bonds (Fig. 2c). Assuming that the surface shell has the thickness of 1 nm, a 10 nm diameter grain contains 25% of its atoms in the surface layer, while a 4 nm grain has already 60% of such atoms. That shows that, in a very small objects (a few nm in diameter), the number of surface-related atoms can exceed the number of the "bulk" atoms.

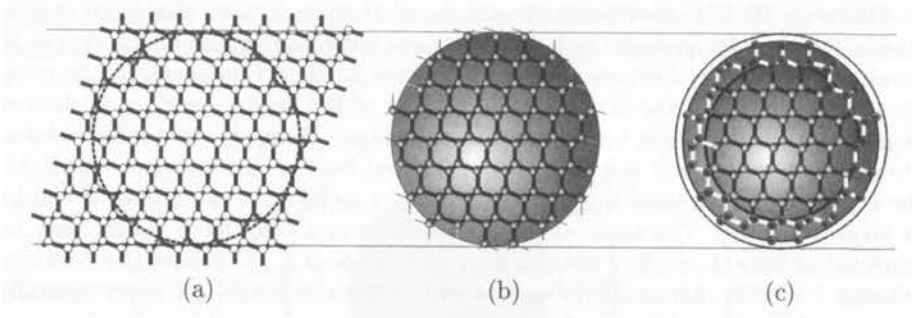

FIGURE 2. Tentative models of the atomic structure of a nanocrystal: (a) single crystal; (b) hypotetical nanocrystal with atoms located at the perfect lattice sites; (c) nanocrystal with a compressed lattice in the surface shell.

Whichever process (reconstruction or generation of strains) dominates, it may be expected to lead to some unique properties of the materials. It may also be expected that the structural changes at the surface propagate to the depth of sev-

eral interatomic distances towards the particle center. Therefore, in a meaningful research on nanocrystals the surface layer (shell) should be treated as a separate structural phase relative to the bulk of the grain (the core).

We believe that the grain surface is a real three-dimensional object that has its own characteristic atomic arrangement. So far, in basic characterization of nanocrystals reported in the literature, the presence of a distinct surface layer is usually ignored. The reason for this negligence is very simple: no information on the specific arrangements of atoms at the surface of nanograins is available and, so far, no experimental methods have been developed for structural analysis of the surface of such small objects. The limitations of some microscopic imaging techniques is demonstrated in Fig. 3. The High Resolution Transmission Electron Microscope (HRTEM) image of a SiC nanograin can discern only the part of the material which has a regular crystallographic structure (c.f. the grain core in Fig. 1) and its atomic planes are perfectly aligned with the incident electron beam. (Note: some electron microscope techniques, like LEED, Tunneling Microscopy, and X-ray diffraction used for the investigation of extended flat faces of single crystals, are not useful for particles like nanocrystals which have very small, irregularly shaped surfaces). *This work presents an analysis of the applicability of powder diffraction techniques for the elucidation of the atomic structure of the surface shell of nanocrystals.*

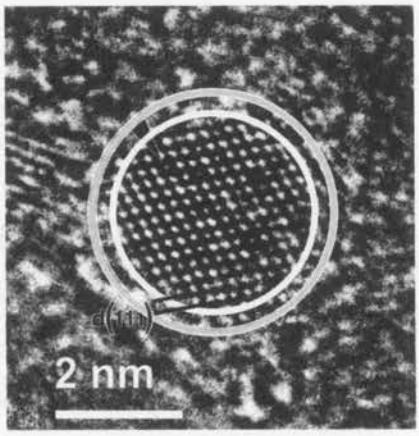

FIGURE 3. HRTEM image of SiC nanocrystal.

Although there is a general understanding in the scientific community that the surface has a significant effect on the physical properties of nanocrystals, the unique properties of these materials are being related to the size of the grains and not to their surface. A number of literature reports on the dependence of different physical properties on the size of nanoparticles exist [9-15]. There is no doubt that changes of physical properties of materials are related to corresponding changes in their atomic structure, what is clearly demonstrated in phase transition processes. Changes of the atomic structure of a crystal are always reflected by the corresponding changes of its lattice parameters. Therefore, while the specific atomic structures of nanocrystals have not been determined yet, changes of the lattice parameters of nanocrystals

(determined from powder diffraction data) relative to those of the bulk crystals have been reported for a variety of nanomaterials. It was also reported that the lattice parameters of a given material depend on the grain size (in metals, Au [16, 17], Al [18], Cu [19], semiconductors like CdSe [20], ionic crystals like NaCl, KCl, NaBr and LiF [21]). Those results were interpreted as "the effect of the grain size on the lattice parameters" and often attributed to the presence of a strong (homogeneous) "internal pressure" caused by the surface stresses (analogous to the surface tension in liquids [22-29]). This "straightforward" interpretation of the experimental findings ignores the fact that the structure of a nanocrystal is not uniform and should be considered either as composed of two distinctive, grain core and shell phases, or as a structure where a large fraction of the atoms at the grain surface is displaced relative to their regular lattice positions (what is equivalent to a presence of strain in the vicinity of the surface). In large (micro-sized) crystallites the number of atoms located at or in the vicinity of the grain surface is orders of magnitude smaller than the number of atoms in the grain core, and their effect on the bulk properties of the materials can be ignored. Also, the contribution of the surface atoms to the diffraction effects measured for such polycrystals in a conventional powder diffraction experiment is negligible. With a decrease in the dimensions of the crystallites down to a few nanometers the number of atoms located at the surface becomes comparable to those in the grain core. Since the surface atoms have a different surrounding and their interatomic distances may differ from those in the bulk material, one set of lattice parameters for a nanocrystal may be inadequate for a unique description of its structure. Conventional diffraction techniques and standard methods of diffraction data analysis are used to characterize the average crystallographic structure of materials through determination of the lattice parameters of the unit cell [30, 31]. These methods are insufficient to detect and quantify small differences between the actual atomic positions in nanograins and those in a regular (unambiguously defined) crystallographic phase. In this paper we show that, although a conventional diffraction experiment is appropriate for characterization of the crystallographic structure of nanosize crystalline powders, the routine methods of the powder diffraction data elaboration may lead to erroneous interpretation of the experimental results. We show that the description of the crystallographic structure of such materials based on the unit cell is erroneous. Accordingly, application of the lattice parameters concept, when used for characterization of the structure of nanocrystals, has to be modified. We suggest a replacement of the lattice parameters, describing the dimensions of the unit cell, by a set of different values of the "lattice parameters", each associated with (determined from) one individual Bragg reflection, and each one at its specific diffraction vector Q. We present the preliminary results of the application of our concept of the *"apparent lattice parameters"* (*alp*) for the elaboration of powder diffraction data of nanocrystals. The concept is demonstrated for nanocrystals with a perfect crystallographic structure, as well as for those with the atomic structure of the surface different than that in the grain core. Some preliminary experimental evidence of the presence of tensile and compressive surface strains in nanocrystalline particles will be shown.

In this work we discuss only the positions of the intensity maxima (i.e. the geometrical aspects of the atomic structure of nanocrystals) through a comparison of the positions of the maxima of the theoretically calculated and experimentally

measured powder diffraction patterns. *We do not discuss the intensities of the Bragg (Bragg-like) reflections*: we assume that all sites are fully occupied (as in a perfect crystal lattice).

2. Powder diffraction

2.1. Experimental techniques

Powder diffraction experiments can be performed using two basic geometries: angular and energy dispersive (Figs. 4a and 4b, respectively). In the more common sense, angular dispersive technique, the diffracted intensity of the monochromatic beam is measured as a function of the diffraction angle (2Θ) with the detector moving around the sample (Fig. 4a). The energy dispersive technique uses a white beam source and the diffracted intensity is measured by a multichannel detector and recorded at a selected, fixed Θ location as a function of the energy of the scattered beam (Fig. 4b). Both techniques can provide equally valuable structural information on the material.

Structural analysis of crystalline materials is performed in two basic steps: (i) determination of the geommetry of the crystal lattice, and (ii) determination of the positions of specific atoms in a representative structural unit (the unit cell). Further analysis can determine the deviations of the crystal lattice from the ideal crystal structure [30, 31]. In this paper we focus our attention on the analysis of the geometry of the lattice of nanoparticles which, as discussed later, requires a more complex description than that sufficient for conventional bulk crystal structures.

The specific form of the Bragg equation depends on whether one uses the angular or energy dispersive geommetry (Figs. 4a and 4b). For a direct comparison of the diffraction patterns obtained using different radiations sources and geommetries we present the diffracted intensities as a function of the corresponding diffraction vector Q (Figs. 4a and 4b).

2.2. Conventional elaboration of powder diffraction data

The simplest information that can be derived from a diffraction pattern are lattice parameters. They are determined routinely based on the Bragg equation which relates the lattice parameters to the characteristic intensity maxima of the diffraction patterns. A common approach to the elaboration of diffraction data is based on the Bragg approximation (Fig. 5). According to Bragg, if a unit cell represents a structure, the structure can be described as a set of infinite, equally spaced parallel planes (Fig. 5). The direction of the scattered beam, 2Θ, is uniquely defined by the relative orientation of the incident beam and the crystal lattice (Θ) and the distance d_{hkl} between the identical atomic planes (Fig. 5). The incident beam is reflected by the atomic planes. There is an unlimited number of families of planes which can be drawn for a given lattice by joining different nodes of the crystal lattice formed by the periodically stacked unit cells (Fig. 6). The planes are denoted by the Miller indices *hkl*. Each family of planes gives a characteristic interference maximum: a *hkl* Bragg reflection located at unambiguously defined position in the Q space (Fig. 7). The locations of the intensity maxima are determined by the specific inter-planar

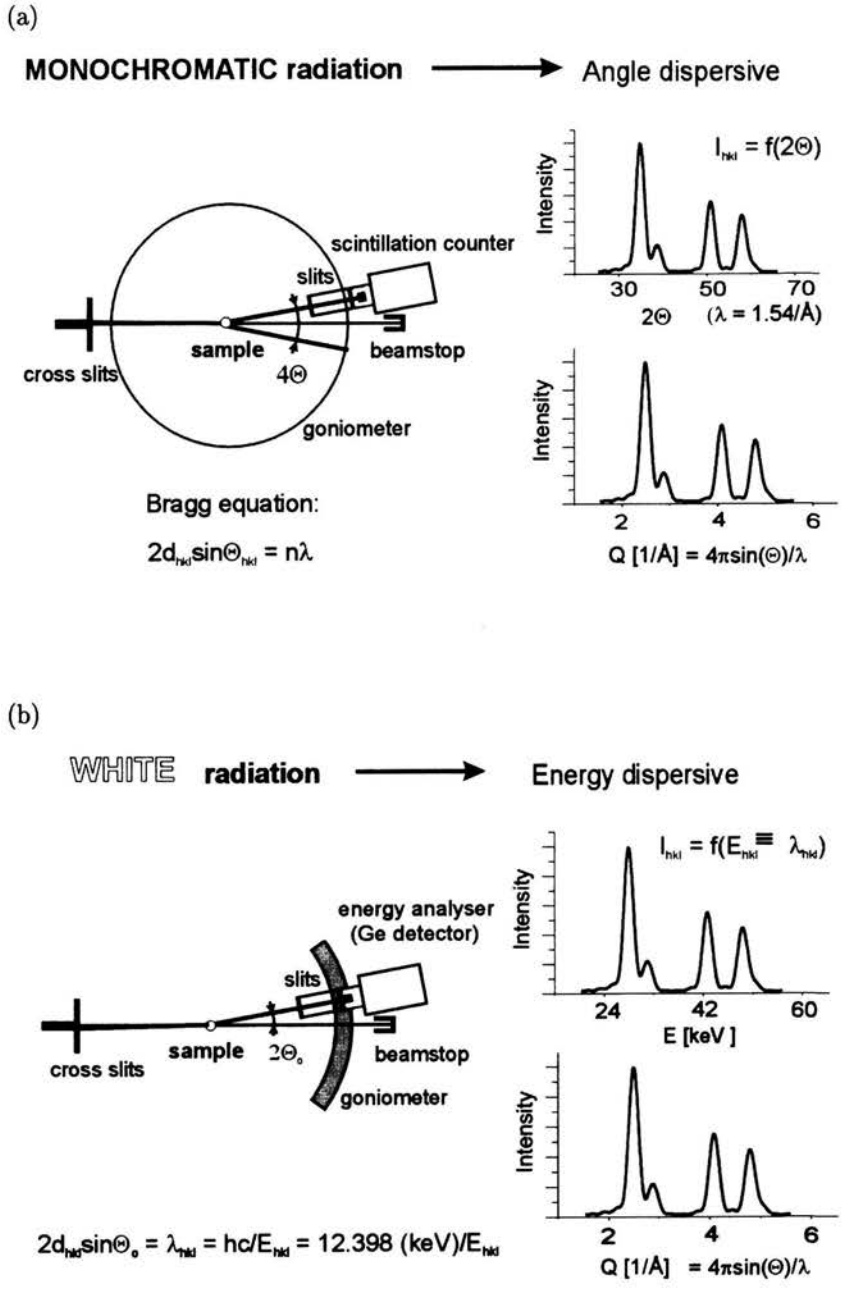

FIGURE 4. Configuration of a powder diffraction experiment: (a) in angular dispersive geometry, (b) in the energy dispersive geometry.

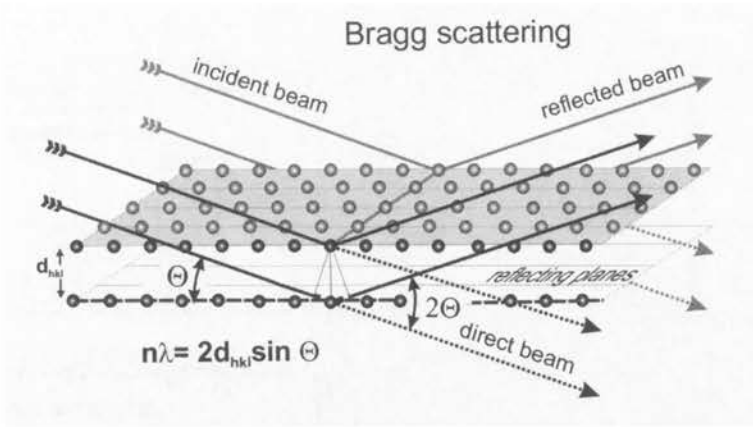

FIGURE 5. Diffraction on a perfect crystal lattice: the atoms are located on ideally flat atomic planes.

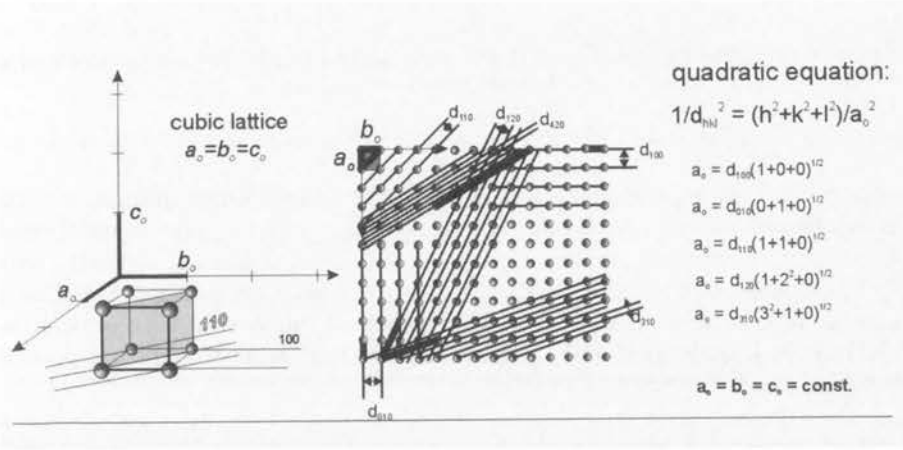

FIGURE 6. Relation of the Miller indices to the (cubic) crystal lattice.

spacings d_{hkl} and the wavelength of the incident beam. Determination of several Bragg reflections (one in the case of a cubic lattice) is sufficient to determine the symmetry, shape and dimensions of the unit cell.

Routine methods of structural analysis of crystalline materials are based on the simple assumption that a unit cell appropriately represents the material structure [30, 31]. To characterize accurately such an atomic structure it is sufficient to determine, (i) the set of the lattice parameters a, b, c, α, β, and γ describing the dimensions and shape of the unit cell, and (ii) the locations of the atoms in the cell, x_i, y_i, and z_i. The complete structural analysis (structure refinement) of polycrystalline samples is routinely done with the powder diffraction technique and elaboration of the experimental data with a crystallographic software like those based on the Rietveld methodology [31]. In the Rietveld method it is assumed that the crystal lattice of the material under examination is uniquely defined by the unit cell. An

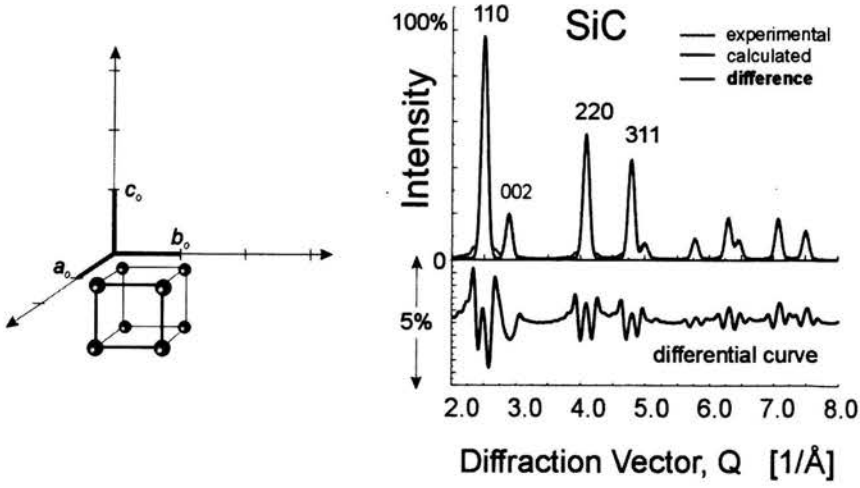

FIGURE 7. Theoretical and experimental diffraction patterns of a SiC polycrystal calculated with the Rietveld refinement program.

appropriate structural model is assumed and the corresponding diffraction pattern is calculated. The theoretical pattern is compared with the experimental results. In an iterative process the structural model is modified and subsequently refined for the best fit of the calculated and measured diffraction patterns based on the selected fit criterion. Figure 7 shows an example of the "best fit" of the theoretical and measured patterns of a SiC polycrystal; the "perfect" fit would correspond to a straight line of the curves differential.

The accuracy of determination of the specific values of lattice parameters and atomic coordinates based on a refinement method like the Rietveld program is dependent primarily on the quality of the experimental data. *The results of such elaboration are accurate if* the fundamental underlying assumptions of a perfect lattice are met, i.e.,

- *the unit cell of the lattice is identical throughout the entire volume of the sample*, and,
- *the latticc is an array of points in space in which the environment of each point is identical to each other.*

These conditions are never strictly met but, for larger crystallites, the deviations from the ideal model are negligible. When the dimensions of the object are comparable to those of the single unit cell the deviations cannot be ignored. In a nanoparticle a large part of the atoms is located at the surface and surrounded differently than those in the core (Figs. 1-3). Thus, a single unit cell cannot represent the entire atomic structure of a nanoparticle. Therefore, the methods of the structural analysis developed for standard crystalline materials may be inadequate for nanosize crystallites.

2.3. The implications of small crystal size for structural analysis by powder diffraction

Conventional methods of the analysis of diffraction data were developed with the assumption that the crystal lattices of real objects are infinite in comparison with the dimensions of the representative structural unit chosen for the material. This assumption is not valid when the dimensions of the crystal are comparable to the size of the unit cell (Fig. 8). For such cases the applicability of conventional methods of the analysis of powder diffraction data (the only diffraction technique that can be used with nanocrystaline materials) needs to be re-evaluated. In our analysis we applied the method of calculation of diffraction patterns introduced in 1915 by Debye [32].

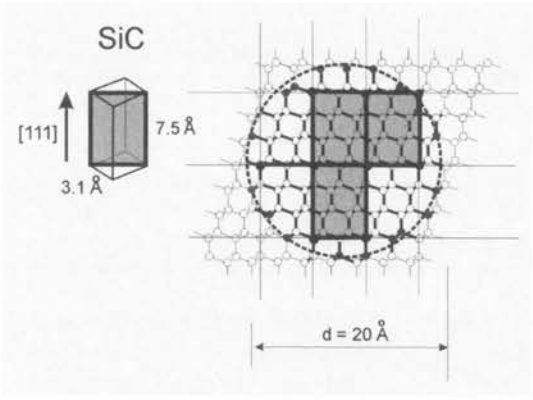

FIGURE 8. Schematic representation of the unit cell in a nanocrystalline grain.

2.3.1. Theoretical calculations of powder diffraction patterns. Relatively small number of atoms forming a nanocrystal provides a unique opportunity to build complete, atom-by-atom, models of small crystals. Using such models and the Debye equations, Fig. 8, the corresponding diffraction patterns can be calculated. Their comparison with the experimental data allows for the evaluation of the atomic structure of nanomaterials.

According to Debye, the intensity of radiation scattered by an array of atoms is the sum of the beams scattered by every pair of atoms, Fig. 9. The intensities $I(\boldsymbol{k})$ of radiation scattered by each pair can be integrated over all spatial orientations of a given crystallite yielding the equivalence of the powder diffraction pattern of a large number of randomly oriented grains. Applying the Debye equation we are able to calculate diffraction patterns for different models of nanocrystalline grains with diameters up to 20 nm without the assumption of a periodic arrangement of the atoms. An important advantage of a direct calculation of the diffraction patterns is that it allows to implement directly into the model different lattice imperfections like strains, point and planar defects, disorderings, etc. For technical reasons, direct calculations of the diffraction effects can be achieved for relatively small arrays of atoms only. A relatively short CPU time, on the order of hours, is sufficient to

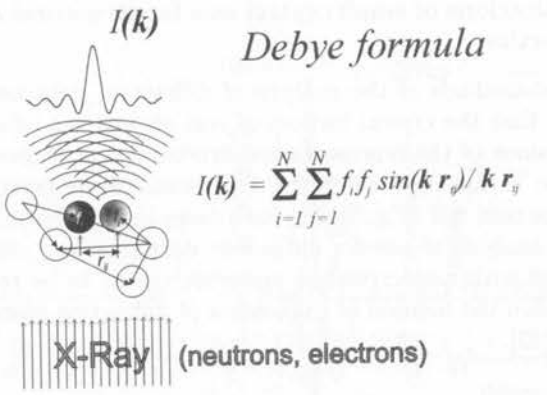

FIGURE 9. Scattering of radiation by an array of atoms; f_i and f_j are the atomic scattering factors of the i-th and j-th atom, respectively, $k = 4\pi \sin\Theta/\lambda$ is the scattering vector, and r_{ij} is the distance between the atoms.

complete one calculation of the diffraction pattern for nanoparticles smaller than 20 nm in diameter [33-34]. For particles with diameter of 25 nm and larger the CPU time is on the order of days and weeks.

2.3.2. Theoretical diffraction patterns of nanocrystals. To verify the applicability of Bragg approach to nanoparticles, we calculated theoretically (using the Debye functions) the diffraction patterns of crystallographically perfect nanocrystals, and calculated back the lattice constant of the model using the Rietveld refinement program. We examined the theoretical patterns calculated for SiC nanocrystals

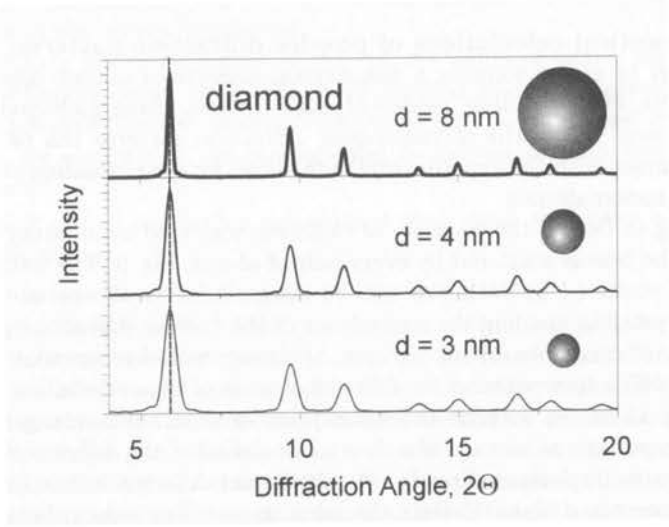

FIGURE 10. Diffraction patterns calculated from the Debye formula for spherical diamond nanocrystals. $\lambda = 0.12$ Å.

with the diameter up to 20 nm. Typical theoretical diffraction patterns obtained for spherical SiC crystallites with a perfect lattice are presented in Fig. 10. Except for the expected widening of the peaks, the patterns resemble those of regular, micro-size powders. However, a detailed analysis of the patterns shows that the calculated intensity maxima are shifted relative to those of the perfect diamond lattice (c.f. Figs. 12 and 15).

In real polycrystalline materials the individual grains have different shapes what leads to changes of the relative intensities of individual reflections. Such "shape effects" are very weak for polycrystals with micrometer size grains, but they can be very strong in small grain powders. The effects of the shape of the crystallites on the diffraction patterns are demonstrated in Fig. 11. Clearly, a change of the grain shape leads not only to a change in the relative intensities of the Bragg reflections but also to a shift of the intensity maxima from the positions corresponding to the reflections calculated based on the unit cell concept. That shows that the positions of the peaks of the powder diffraction pattern of nanosize crystallites may not match those of the Bragg lines.

The best verification of any method proposed for elaboration of experimental results is an application of the method to a "perfect experimental data". In our case the experiment is simulated by calculating a perfect diffraction pattern using the Debye functions (c.f. Sec. 2.3.1).

The elaboration of any diffraction data has to account for two groups of parameters: instrumental and sample-dependent. Our virtual "perfect experiment" does not require any instrument-related corrections. However, in a real laboratory practice the experiments are not perfect and any instrument/geometry imperfection is

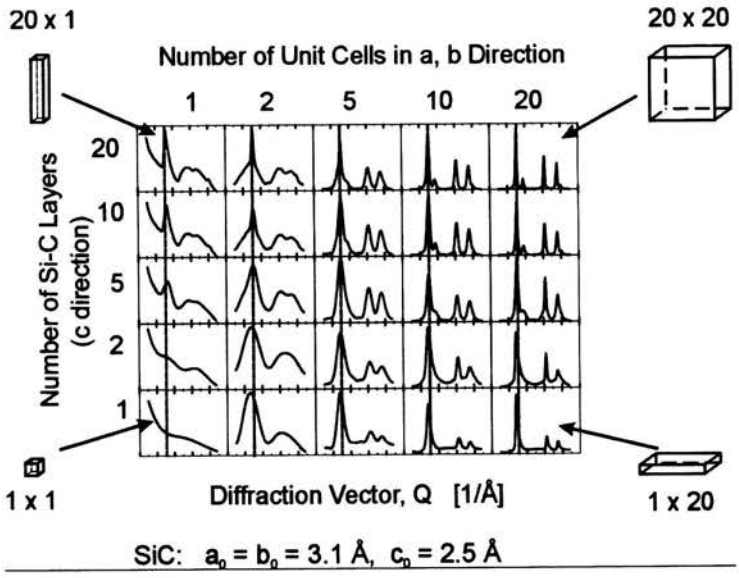

FIGURE 11. Theoretical diffraction patterns calculated from the Debye functions for SiC nanocrystallites of different shape.

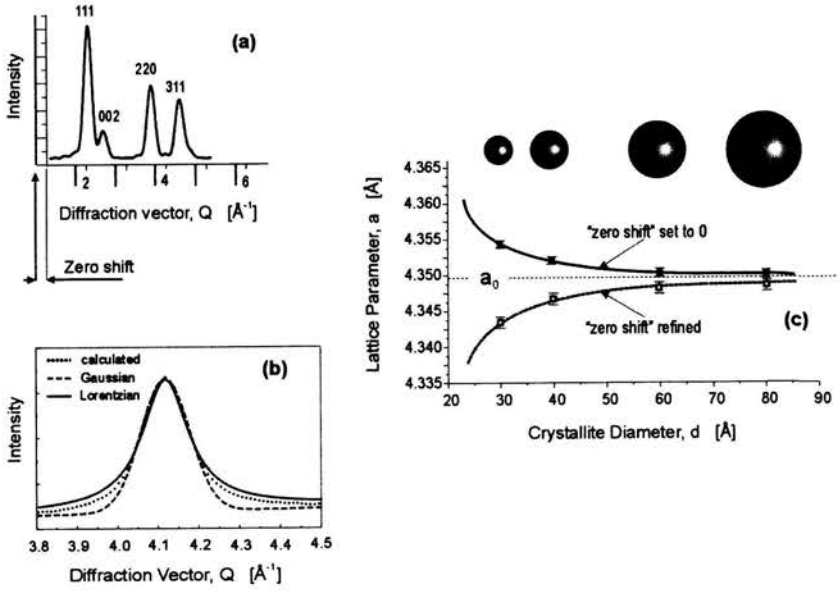

FIGURE 12. The results of theoretical calculations of the diffraction effects in nanocrystals of SiC. Lattice parameter of the model, $a_0 = 4.350$ Å. (a) a typical theoretical diffraction pattern; (b) a representative shape of the diffraction peaks; (c) lattice parameters back-calculated from the theoretical diffraction patterns for different size particles. Full symbols and solid line – the refinement made w/o correction for the "zero shift"; open symbols and dotted line – the refinement made w/correction for the "zero shift".

a source of errors. These instrument imperfections lead to the so called "zero shift" effect: the real beginning of the diffraction pattern is usually shifted relative to the apparent "zero" position of the experimental set-up (Fig. 12a) with the obvious consequences for the accuracy of the experimental results. Standard data elaboration routines (c.f. Sec. 2.2) evaluate and correct the pattern for the "zero shift" factor.

The second type of experimental errors is due to the properties of the sample itself. The Bragg diffraction relations apply to infinite size crystals and in a model experiment all diffraction peaks have the Gaussian-type shapes. For small crystallites the shape of the peak is no longer Gaussian but a combination of Gaussian and Lorentzian functions (Fig. 12b). Our calculated diffraction patterns were analysed applying the Rietveld methodology assuming that the reflections have shapes that are a combination of these two basic functions. We used two procedures of the elaboration of our diffraction data:

1. Perfect experiment

In this method, consistent with the "perfect experiment" approach, we didn't apply the procedure that corrects for the experimental/instrument imperfections. We refined the as-calculated diffraction data releasing only the lattice parameters and the line shape. The line shapes were fitted using the pseudo-Voigt function.

The calculated values of the lattice parameter for different sizes of the particles are shown in Fig. 12c (full symbols, solid line). Obviously, the procedure yields the lattice parameters different than that of the starting model. In addition, it generated an artificial "*dependence of the lattice parameter on the size of the particle*".

2. Imperfect experiment

In this case we treated our calculated diffraction data as if they were obtained experimentally and, so, required a correction for the instrument imperfections. Therefore, we refined the lattice parameters releasing the "zero shift" correction in the Rietveld program. The results of this calculation are shown by the open symbols/dashed line in Fig. 12c. As we can see, the "zero shift" correction procedure generated another artefact: despite no real instrumental errors introduced to our model diffraction pattern, the program lead to a change in the value of the calculated lattice parameters relative to the model input value. The effect is apparently even stronger, and opposite in sign than that in the first procedure, so the combined result generates the "*dependence of the lattice parameter on the size of the particle*" in the opposite direction.

As seen from the above, a mathematically correct, commonly accepted, and widely used *Rietveld refinement program yields erroneous results*: the lattice parameter back-calculated using this procedure generated an artefact – "a dependence of the lattice parameter on the grain size". The magnitude of this superficial effect decreases with an increase in the grain size and can be ignored for crystallites 10 nm in size or larger (Fig. 12c). The reason for those effects is the non-compatibility of the assumption used in derivation of the Rietveld methodology (infinite atomic planes) and the real nature of the crystals (finite size of real particles). This effect is negligible for micron-size and larger crystals. The above limitation of applicability of the Rietveld method has apparently been overlooked by many researchers and might have led to incorrect interpretation of the diffraction data of nanomaterials. Our analysis shows that application of routine methods of elaboration of diffraction data requires a very critical assessment of the results. In particular, internal standard should be used to prevent the apparent errors introduced by the "zero shift" correction routine during elaboration of any diffraction results. This is particularly important for crystallites as small as several nanometers.

3. "Apparent lattice parameters" – a novel method of powder diffraction analysis

Diffraction pattern is a projection of the atomic structure of the material existing in the real space into the reciprocal space [32]. Structural analysis based on a diffraction data is in fact a conversion of the information on the atomic structure collected in the reciprocal space (the pattern) into the real space (the atomic model). The methods of elaboration of the powder diffraction data, through the Bragg equation or the Rietveld refinement programs, are in fact the methods of transformation of the experimental data from the reciprocal to the real space. We showed in Sec. 2.3.2 above that these methods, which work well for conventional polycrystalline materials, do not apply in full extend to nanocrystals. Below we ex-

amine in some details the shortcomings of the conventional elaboration techniques with respect to nanocrystals, and propose a new approach to the analysis of powder diffractograms of nano-powder materials.

A dependence of the results obtained with the Rietveld program on the crystallite size is apparently the effect of the shifts of the positions of individual Bragg reflections relative to those corresponding to the perfect lattice. As discussed in Sec. 2.2 above, this phenomenon is caused by the approximation of the crystal lattice by a set of infinite atomic planes, which is not justified for nanosize crystals. As a consequence, the Bragg reflections cannot be assigned to a unique value(s) of the lattice parameter(s) so the term "lattice parameter" loses its fundamental meaning. Our analysis of these phenomena discussed in Sec. 2.3.2 lead us to a conclusion that the effect of the limited number of atoms in individual nanograins on the diffraction pattern is different for different reflections. As a result, the individual peaks are incoherent to each other ("coherence" means that all Bragg reflections obey the quadratic equation for a single, unique set of the lattice parameters, c.f. Fig. 6) and the diffraction pattern evaluation programs that assume coherency lead to erroneous results. Since the lattice parameters calculated from different Bragg reflections are not invariant, we developed a new approach to the analysis of such diffraction data based on individual diffraction peaks. For a given Bragg reflection *hkl* (at the diffraction vector Q) we calculate the corresponding value of the lattice parameter that we call the "apparent lattice parameter" (*alp*).

> *Note:* We showed in Sec. 2.3.2 that the quadratic equation, used routinely in every conventional crystallographic program and which serves for refinement of the lattice parameters, is not valid for very small crystallites. Consequently, such an equation cannot be used to calculate the lattice parameters even if the atomic structure of the crystallite has a perfect crystal lattice with three-dimensional periodicity and a unique set of lattice parameters. That means, that the methods of diffraction data elaboration based on the Bragg approximation fail: using the Bragg approach and the quadratic equation we are unable to obtain the correct information on the atomic structure of a nanocrystal. Under such circumstances the term "Bragg reflection" should, then, be replaced by the term "Bragg-like reflection".

We propose the application of the *Bragg approximation* and of the quadratic equation for derivation of d values calculated *separately for each individual reflection.* In this way we *associate the calculated d-values with the specific values of the diffraction vector Q of a given reflection.* From the as-calculated d-values we derive the corresponding values of the lattice parameters which we call the "apparent lattice parameters". With this procedure we obtain not a unique set of values of the lattice parameters but a set of the *alp* values and their corresponding diffraction vectors Q. (For the sake of simplicity, we illustrate our methodology based on cubic lattices, i.e. the structures defined by only one lattice parameter. In a general case, derivation of a set of three independent *alp* values corresponding to three lattice parameters a, b, c is necessary.) In addition to calculations based on individual Bragg reflections we can also calculate the *alp* values for a group of several adjacent Bragg reflections in the selected range(s) of the Q-values. Such procedure is very useful in the case of a strong overlapping of the reflections, particularly in the large Q range.

The results of the evaluation (using the Rietveld program) of the theoretical diffraction pattern computed for a model of cubic SiC crystal of 8 nm in diameter for different Q-ranges are shown in Fig. 13. The diffraction pattern of the SiC nanocrystal calculated from the Debye functions and that calculated by the Rietveld program (solid and dashed lines, respectively) are shown in Fig. 13a. The difference between these two patterns (Fig. 13b) is up to 5% of the maximum intensity of the (111) reflection (Fig. 13b). This is a very large discrepancy, particularly given the fact that both curves were calculated theoretically for the same, perfect-lattice crystallographic model. The difference between these two calculations is, that the

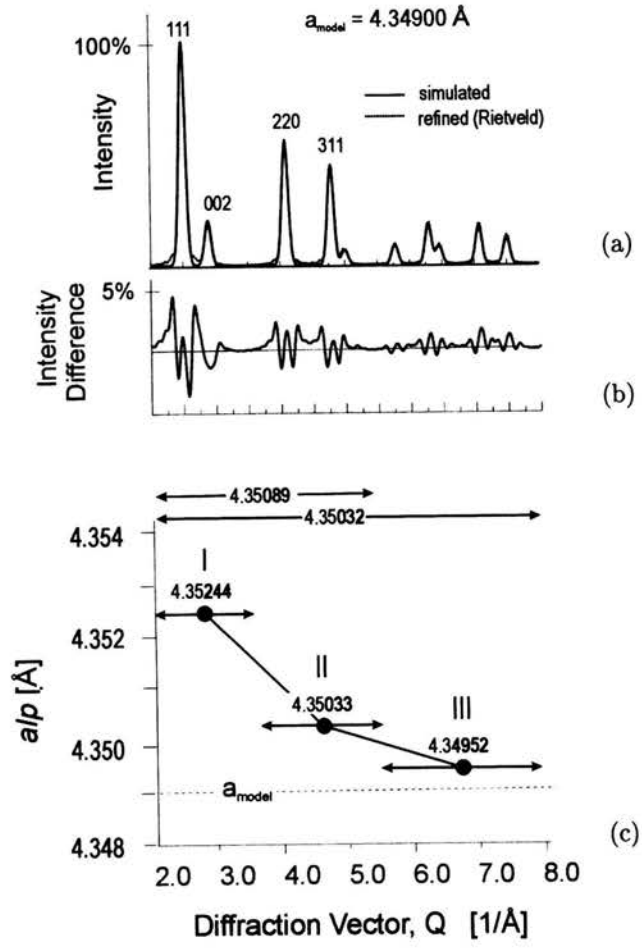

FIGURE 13. *Alp* values calculated from the theoretical diffraction pattern of SiC nanocrystal of 8 nm in diameter. (a) solid line – as-calculated diffraction pattern; dotted line – the pattern refined with the Rietveld program; (b) difference in intensity between the as-calculated and refined diffraction patterns; (c) *alp* values calculated for different ranges of the diffraction vector Q.

Rietveld program assumes that the crystal is infinite and is uniquely represented by the unit cell, while the Debye method accounts only for the existing atoms in the model of the crystallite. The positions of the reflections calculated by the Rietveld program correspond to a perfect crystallographic lattice with one lattice parameter a common for all positions of the Bragg reflections, in accordance with the quadratic equation. The Bragg-like lines calculated from the Debye functions are shifted relative to those corresponding to the Bragg reflections of the "perfect and infinite lattice". This is the main reason of the discrepancy between the patterns shown in Fig. 13b: the Rietveld program finds a single lattice parameter which gives the best fit to all Bragg reflections of the pattern. The program has no option to fit individual Bragg reflections. The lattice parameter refined by the Rietveld program is a compromise (the least squares best fit) which is to minimize the discrepancy between the experimentally measured (here: calculated by the Debye functions) and the theoretical pattern of the unit cell used by the Rietveld program. The additional reason for the discrepancy between the patterns is a complex shape of the Bragg-like reflections of nanocrystals. The Bragg reflections of a uniform-size-grain crystalline powder should have a Gaussian shape. The shift of the Bragg-like reflections of nanocrystals is accompanied by a distortion of the peak symmetry. No simple analytical function describing the shape of the calculated reflections exists. In the Rietveld program we used symmetric line shape functions: Lorentzian, Gaussian and their combination (pseudo-Voigt and Pearson functions).

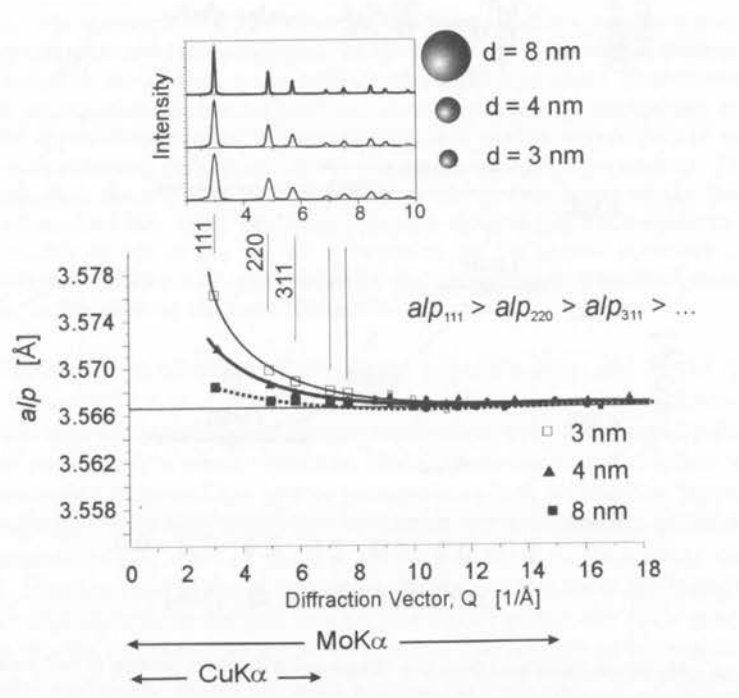

FIGURE 14. *Alp* values calculated from individual Bragg reflections of the theoretical diffraction patterns of spherical diamond nanocrystals of 3, 4 and 8 nm in diameter.

Figure 13 illustrates the inadequacy of the standard methods for evaluation of diffraction patterns of nanomaterials. The calculated values of the *alp* parameter for different Q-ranges are shown in Fig. 13c. The lattice parameter as-refined for the whole calculated pattern (what is equivalent to the *alp* parameter computed for the entire diffraction spectra) is 4.35032 Å. This value is larger than the lattice parameter of our model, 4.349 Å, $\Delta a/a_0 = 0.03\%$. The *alp* value obtained for small Q-values (range I) is larger (by 0.08%) from that of the model, as are the *alp*'s calculated for greater Q values. The difference between the as-refined *alp*'s and the real a value decreases with the increase of the scattering vector Q. The *alp* values plotted versus the diffraction vector Q follow a monotonic curve which tends to reach the real a value at large diffraction vectors (Fig. 14). To derive the a value of the crystal lattice of very small crystallites, diffraction patterns obtained at very large Q's are necessary.

From the above (Figs. 13 and 14) it follows, that for a nanocrystal with a perfect, uniform structure its lattice parameter can be derived from powder diffraction patterns using two methods:

1. a refinement of the real lattice parameters using only the part of the pattern with large Q-values (above about 10 $Å^{-1}$ for grains of several nm in size), or,
2. a determination of the *alp* values for different reflections and matching them with the results of the theoretical predictions obtained for appropriate models. This method requires the knowledge about the grain size distribution function, which is usually known only approximately.

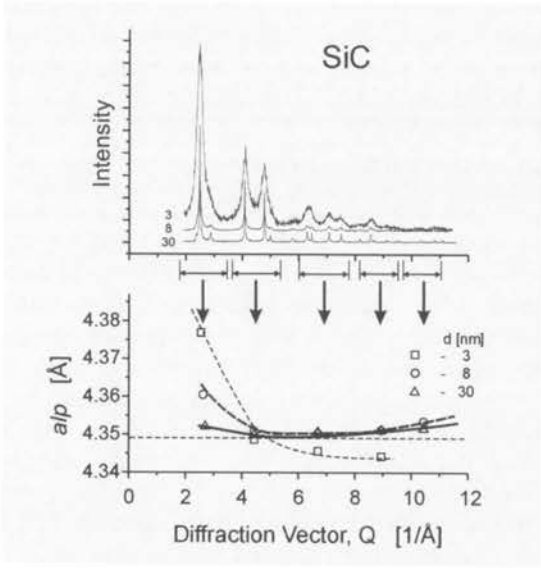

FIGURE 15. Experimental diffraction patterns of nanocrystalline SiC powders with average grains of 3, 8 and 30 nm in diameter (upper graph) and their corresponding *alp* plots (lower graphs). The measurements were performed at powder diffractometer at SNBL Station, ESRF, Grenoble, with $\lambda = 0.7$ Å radiation source.

A series of our powder diffraction experiments performed in a large Q range for nanocrystalline SiC, diamond, and GaN particles showed, that the type of the *alp-Q* relations derived for models of nanocrystals with a perfect crystal lattice is similar to the experimental ones. Examples for SiC nanocrystals are given in Fig. 15. However, the measured shifts of the Bragg reflections from their proper (i.e. expected for a unique and crystallographically uniform structure) positions are much larger (particularly for small Q's) than those calculated for nanocrystals with a perfect (unstrained) lattice (Fig. 15): for the (111) reflection and 8 nm diameter grain the discrepancy is 0.23% as compared to 0.08% for a perfect SiC nanocrystal (Fig. 13c). This implies that the crystallographic structure of nanocrystals is not a uniform perfect lattice such as the one in the bulk material; a nanocrystal is more than just a small single crystal. Accordingly, more complex models of the particles need to be used to evaluate the structure of real nanograins. Therefore, in our further study, we applied the concept of the *alp* parameters for models with a strain in the surface shell of the grains.

4. Surface strain in nanocrystals

Non-uniformity of the atomic structure of nanocrystals is obviously caused by the surface of the grains being either reconstructed or under stress. Two different approaches to the study of non-uniformity of the nanograin structure can be taken: investigation of the surface properties, or modelling of the surface structure. In this work we analyse the atomic structure of nanocrystals (with reference to) based on the general concept of the presence of a surface tension in small liquid droplets and surface stresses in solid particles. A strain present at the surface of small particles is expected to create an internal pressure inside the grain. In this work we assume that the strains are not confined to the outmost layer but propagate to some distance towards the center of the particle.

4.1. The concept of the surface free energy

The theory of surface tension has been developed for liquids but, with some modifications, can also be applied to solids as well [6, 15, 22-24, 26, 27, 29]. For solids, the presence of free bonds (dangling bonds) is called the surface stress and/or surface free energy. In liquids, where atoms/molecules are very mobile, they can migrate from the bulk of the fluid to the surface and, at equilibrium, the optimum (minimum energy) shape of the phase is assumed. The difference between the surface tension γ and the surface stress is, that while the former is a measure of the work required to *create* an extra surface area, the latter is that of the work that was required to *deform* the surface. Because the mobility of atoms in solids is much lower than that in liquids, a change of the shape of the solid can be ignored and only local strains in the vicinity of the surface need to be considered. The strains can force a reconstruction of the surface [15, 22, 23], but such reconstruction is confined to the local atomic configuration only. The actual atomic structure of a crystallite (of its interior and surface) is a compromise between:

- a tendency to reduce the total surface area of the particle (a tendency to adopt the spherical shape, [35]), and,

- a tendency to reduce the total number of the broken bonds at the surface (a tendency to flatten the surface demonstrated by the enlargement of the crystal facets with the lowest free energy at the expense of those with higher ones).

A quantitative description of the surface free energy in solids is very complex. Evaluation of the influence of the surface effects on the atomic structure of a particle can be done using a Laplace-type law keeping in mind, however, that a derivation of the surface tension coefficient γ from the lattice contraction is not fully applicable to solids. The common drop model used in the Laplace Law suggests that an internal pressure is generated inside the liquid droplet:

$$\Delta P = \frac{2\gamma}{r}. \tag{4.1}$$

Crystallites have facets, their lattice is anisotropic, and the surface stress is not uniform. Nevertheless, the concept of the internal pressure can still be applied to the interior of small crystals assuming that the elastic properties of the material are isotropic and the particle is spherical in shape. Applicability of the Laplace Law to a solid is better when the crystal is surrounded by a liquid or gaseous phase and can exchange mass with the environment by dissolution/deposition or evaporation/condensation processes. Experimental evaluation of the surface stress in small solid particles doesn't have a standard, commonly accepted measurement technique, although the results of some studies on the subject have been reported in the literature [17, 20, 25].

The change of the surface energy (γA, where A is the surface area) can be described by:

$$d(\gamma A) = \gamma\, dA + A\, d\gamma. \tag{4.2}$$

The surface stress coefficient is defined as

$$\boldsymbol{f} = \gamma + A\frac{d\gamma}{dA}. \tag{4.3}$$

From this relation it follows, that the surface is in a state of dilatation or contraction depending on whether the surface stress $\boldsymbol{f}$ is greater or smaller than the surface tension [6, 17]. Principally, it should be possible to determine (from the change of the lattice parameters of the interior with a change in the grain size, i.e. from the compressibility of the crystal lattice of the grain core) the strain present in the surface layer using the Laplace Law. For a surface that has two principal radii of curvature, r_1 and r_2,

$$\Delta P = \boldsymbol{f}\left(\frac{1}{r_1} + \frac{1}{r_2}\right). \tag{4.4}$$

It can be shown that generation of a high internal pressure in nanocrystals results from their small size and not directly from their surface curvature. For example, the internal pressure in a cube-shaped particle equals $2\boldsymbol{f}/l$, where l is the length of the cube edge (Fig. 16).

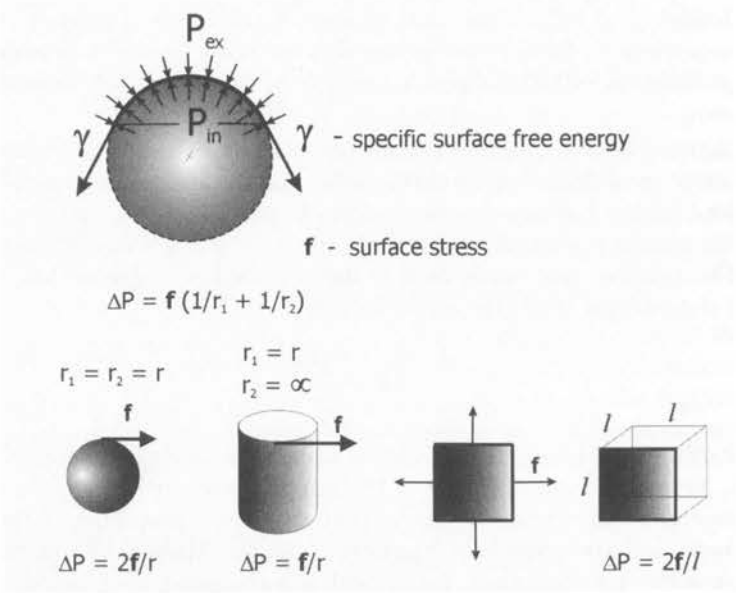

FIGURE 16. Internal pressure in a solid particle due to the presence of surface stresses.

A presence of an internal pressure in the interior of a particle should be detectable through the corresponding change Δa of the lattice parameter a. In a small crystal of radius r this change can be expressed as a function of $\boldsymbol{f}$:

$$\frac{\Delta a}{a} = \frac{3}{2}\frac{r\boldsymbol{f}_{rr}}{B_0} \tag{4.5}$$

with $\boldsymbol{f}_{rr}$ the "mean" surface stress in the radial direction, r the particle radius, and B_0 the bulk modulus. An appropriate experiment designed to evaluate the surface stress would then measure the contraction of the crystal lattice as a function of the particle size. The surface stress coefficients were calculated for nanocrystalline Au and Pt powders based on the electron diffraction measurements of the lattice parameters [17]. It was found that for both materials the as-determined surface stresses are slightly larger than those corresponding to the surface tension calculated from the broken bond model [25]. It has been suggested [17] that the distances between the atoms at the surface are slightly greater than those corresponding to the minimum energy potential. This result is in fact a confirmation that a surface relaxation took place and the surface of Au and Pt particles is under tension. Studies on relaxation of the atomic structure of nanosize crystallites of CdSe using the electron diffraction technique showed [20] that the value of the surface energy calculated from the lattice compression varies with the particle size. The surface energy was found to be smaller than that in the bulk single crystal for the same atomic plane (0.34 compared to 0.55 N/m). It was concluded that this difference is a function of the surface passivation by bound species and/or by a reconstruction that might have occurred on the nanocrystal surface. Additional parameter which could be useful in studies on the surface energy and surface stress is the environment

surrounding the particle: different media, gas, liquid or solid may affect the surface tension to a different degree. No systematic studies of that type have, however, been reported yet.

The theory of surface tension has been developed for continuous media. The theory does not concern any specific atomic structure of the surface and, also, it ignores the non-tangential components of the surface stresses present in real materials. In nanomaterials, where the size of the grains is not much larger than the single inter-atomic distances, the surface cannot be considered as being a smooth layer surface which surrounds a certain liquid or solid volume and has a zero thickness. In a nanograin the surface stresses are located at the particle face and its vicinity, so one should talk about a surface shell rather than a two-dimensional surface assumed in the theory of the surface tension.

4.2. Effect of a presence of surface strain on *alp*

According to the Laplace-type law the lattice of a nanograin core can either be expanded or compressed hydrostatically (relative to that in large crystals) due to the presence of the surface free energy [22-29]. Based on the above we assumed, that the structure of the grain core is uniform and can be described unambiguously by the space group and the lattice parameters.

The surface structure is not clearly defined and we can apply only conceptual models of the nanoparticle surface layer, for example:

(a) The structure of the surface shell of a nanograin resembles that of the grain core: it has well defined thickness, symmetry, and interatomic distances;

(b) A radial strain field exists in the vicinity of the surface: the interatomic distances decrease or increase from the surface towards the particle center;

(c) The atomic structure of the surface is randomly disordered (forming a glass-like phase).

In models (a) and (b) a presence of long range ordering of the surface atoms is assumed, while in model (c) only a short-range order in the surface layer is present. In any case, the surface is a "low dimensional structure" and has a defined thickness, but it also contains strains and, thus, cannot be unambiguously defined and represented by a unit cell parameters. No experimental methods, which would allow for a direct analysis of such complex structures of nanocrystals, are available at this moment [36-38]. The analysis of the conditions required for ordering of atoms in three-dimensional crystal lattices, and application of the general theory of the origin of the surface strain from the internal pressure in the grain interior could be helpful for predictions of the surface structure of nanocrystalline grains. No general theory or model of the surface of nanocrystals is available yet.

In this work we applied the model of a nanocrystal where the grain core has a uniform crystallographic structure and is unambiguously characterized by the lattice parameter a_0. We assumed that the atomic structure of the surface is strongly correlated with the parent structure of the grain: it is basically the structure of the core but centro-symmetrically deformed, compressed (Fig. 17) or expanded due to a presence of the surface strain. According to the model, the term "lattice parameters" may not be applied to the whole nanocrystal nor to the surface layer. No

common, specific interatomic distances can be assigned to the surface shell. However, to simplify the description of the model, we introduce the parameter a_s which corresponds to the interatomic distances at the outmost atomic layer of the particle (Fig. 17). Assuming that the arrangement of the atoms in the surface shell is similar to that in the grain core, the value of a_s can be expressed as a fraction (in %) of the lattice parameter a_0. The actual values of the interatomic distances within the surface shell can be expressed as a function of the distance from the particle center and vary between a_0 in the grain core (at distances $r < R_0$) and $a_s = a_0 \pm \Delta a$

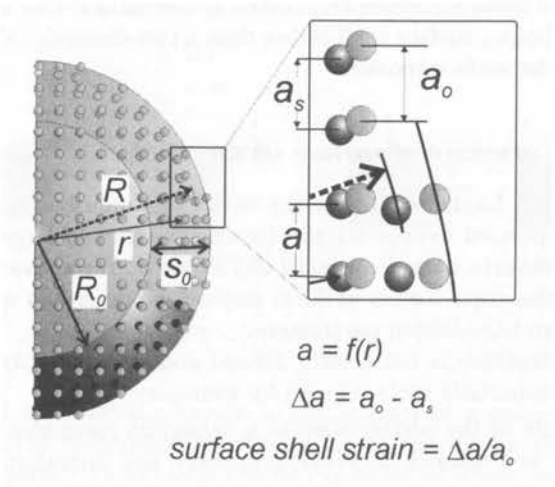

FIGURE 17. Tentative model of a nanocrystal with strained (compressed) surface layer. R_0 – radius of the core; R – radius of the grain; s_0 – thickness of the surface layer; r – distance from the center; a_0 – interatomic distance in the relaxed lattice; a_s – interatomic distance at the surface.

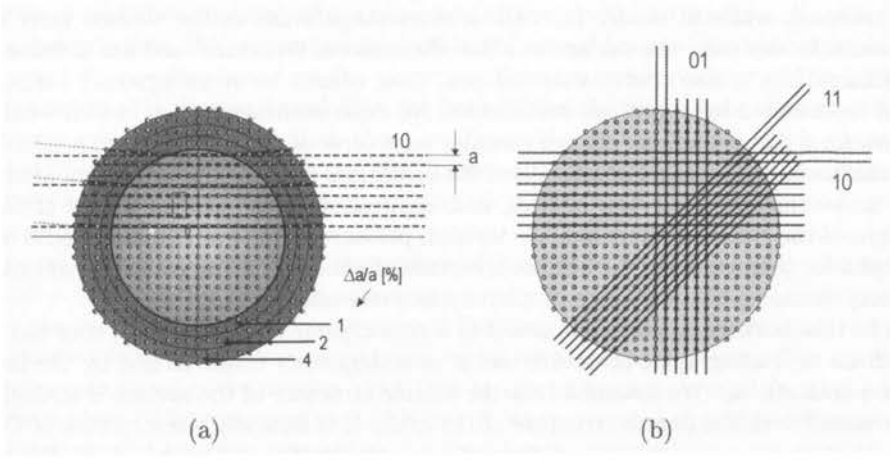

FIGURE 18. Schematic representation of cubic nano-structures: (a) grain with strained (expanded) surface shell; (b) grain with uniform, perfect lattice.

(for $r = R$). The sign in front of Δa depends on whether the surface is compressed ($-$) or expanded ($+$) relative to the grain core. The ratio $\Delta a/a_0$ is quantifying the surface strain.

Our model of a cubic lattice nanoparticle with and without the tensile strain in the surface shell is shown in Figs. 18a and 18b, respectively. A presence of strain in the grain surface layer, the surface shell, leads to a deformation of the atomic planes (Fig. 18a). As shown in the figure, the atomic planes lose their planarity and mutual parallelity. As a consequence the interplanar spacings in such nanocrystals lose their unambiguous meaning. Also, the conventional description of a crystal lattice based on the definition of a unit cell cannot be applied to the whole crystallite although it still can be used for the description of the grain core structure. A diffraction on such crystal-like objects may not be based, however, on the Bragg approximation: the concept of interplanar spacings is meaningless for non-planar (bent) surfaces. However, for the sake of convenience and consistency with the description of the diffraction effects on nanocrystals having a perfect crystal lattice (c.f. Secs. 2.3.2 and 3) we use the classical description of the diffraction patterns also for our *alp* concept. The diffraction patterns calculated for the models of an 8 nm diameter SiC nanocrystals with a tensile, none, and compressive uniform strain in the surface shell ($\Delta a/a_0 = \text{const.}$) are shown in Figs. 19a, 19b, and 19c, respectively. The strain in the surface shell shifts the positions and changes the symmetry of the Bragg reflections. Since asymmetric peaks do not have uniquely defined positions, those were determined based on the location of both the maximum and the weighted

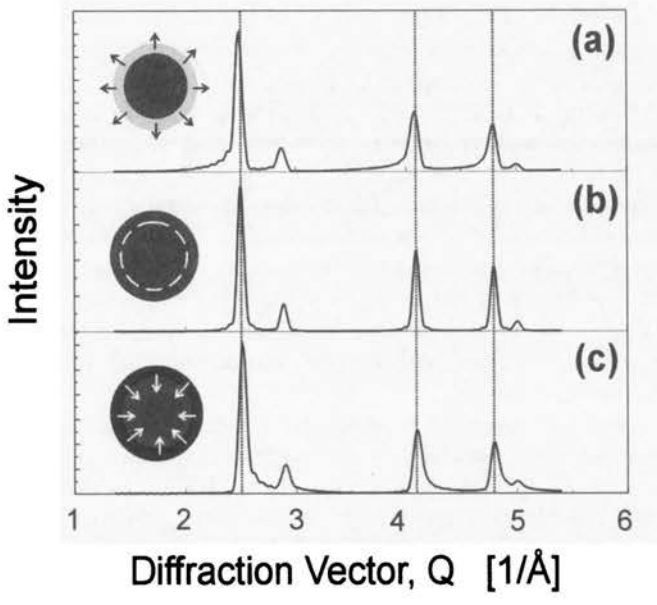

FIGURE 19. Diffraction patterns of a 8 nm SiC grain with the surface shell of 0.7 nm in thickness, calculated for different magnitudes of strain in the surface layer: (a) $\Delta a/a = +10\%$; (b) $\Delta a/a = 0\%$; (c), $\Delta a/a = -10\%$.

center of the individual reflections. The character of the dependence of the calculated *alp* values on Q is similar for both methods, although specific values of Q are somewhat different.

5. *Alp* analysis of powder diffraction data

For low strains in the surface shell the asymmetry of the Bragg reflections is very small and can be ignored. Figure 20 shows experimentally measured (220) reflections of microcrystalline (Fig. 20a) and nanocrystalline (8 nm in diameter, Fig. 20b) SiC powders together with the Lorentzian and Gaussian shape curves. While the shape of the microcrystalline powder reflection matches closely the Gaussian function, that of the nanocrystal corresponds to a combination of the Gassian and Lorentzian fuctions. To determine the *alp*-Q relation for our theoretical and experimental patterns, the diffraction peaks were fitted using a standard shape function (pseudo-Voigt) available in every Rietveld program. The examples of Bragg-like reflections (111 and 246) calculated for 6 and 12 nm diameter SiC nanocrystals are shown in Figs. 21a and 21b, respectively. The patterns were calculated both for models with a relaxed, perfect lattice and for nanocrystals with a strained surface shell. Both the shapes and positions of the reflections change with the grain size, a presence of strain, and the diffraction vector Q (Fig. 21). That applies to reflections both at low (111) and high (246) Q values (Fig. 21).

(220) reflections obtained experimentally for SiC of different grain size are shown in Fig. 22. The position of the peak changes with a change in the grain size. In terms of the absolute values of the diffraction angle the shifts are very small and a standard diffraction equipment is insufficient to discern such minute differences in the positions of the Bragg reflections. The patterns presented in Fig. 22 were collected at the BW5 station at HASYLAB, DESY, Hamburg in the angular dispersive geometry with a very small Θ step of only 0.003° and using the 0.12 Å synchrotron source. Precise diffraction data require a very precise alignment of the system and necessitate also the use of an internal standard to obtain very accurate correction for the instrument "zero shift". The combined effect of the high precision experiment equipment and advanced numerical elaboration of the diffraction data (c.f. Sec. 3) allowed for the precision of our determination of the diffraction maxima on the order of 0.0003 Å. A higher precision can be achieved using longer wavelength of the incident beam, but combined with a simultaneous reduction in the experimentally available Q-range (see below).

Table 1 gives the values of representative quantities for the elaboration of a powder diffraction data obtained in the angular dispersive geometry. The values are given for low ($Q = 2.5\,\text{Å}^{-1}$) and large ($Q = 10.8\,\text{Å}^{-1}$) diffraction vectors (111 and 246 Bragg reflections, respectively). As discussed in the previous sections, for the purpose of a conclusive analysis of the *alp*-Q relations the diffraction patterns obtained for large Q-values are necessary. On the other hand, the positions of the Bragg reflections should be measured with very high accuracy: the shifts of the Bragg lines caused by the small size of the crystallites and a presence of strain are very small (Table 1). These two conditions cannot be satisfactorily met in a single diffraction experiment. To obtain a diffraction pattern in a wide range of Q, a short

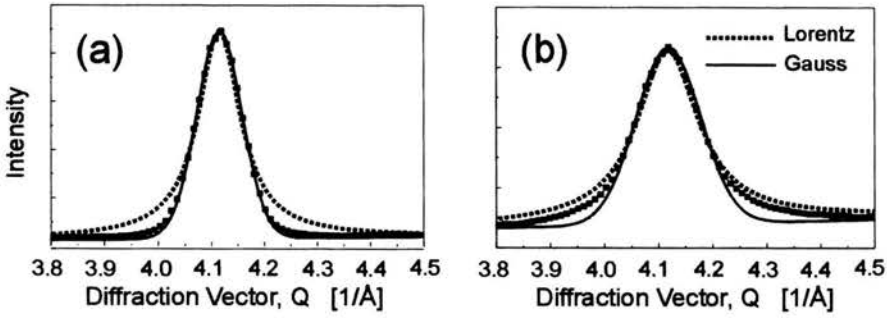

FIGURE 20. Shapes of experimentally measured (solid points) 220 Bragg reflections and Gaussian and Lorentzian functions: (a) microcrystalline powder; (b) nano-crystals.

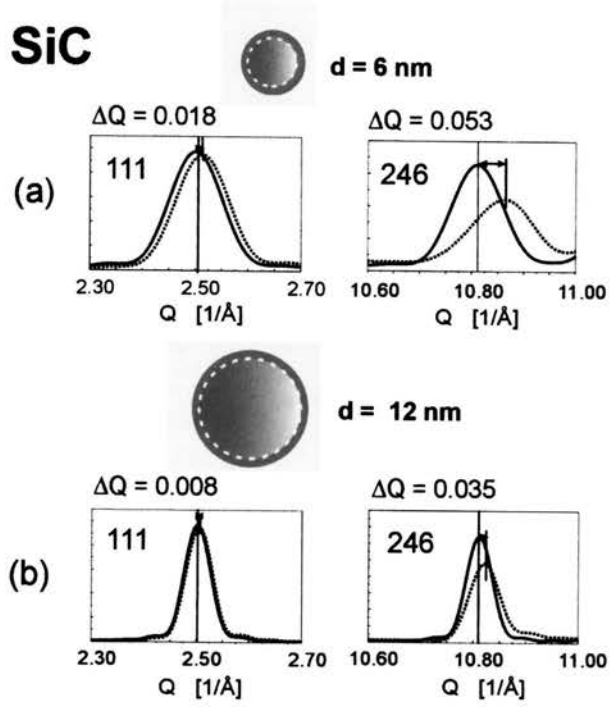

FIGURE 21. Bragg-like intensity curves calculated for models of SiC nanocrystals with a relaxed lattice (solid lines) and compressed surface shell (dotted lines) for two different reflections, (111) and (246): (a) grain diameter 6 nm; (b) grain diameter 12 nm. The thickness of the surface shell, s_0=0.7 nm, the strain $\Delta a/a_0 = 5\%$.

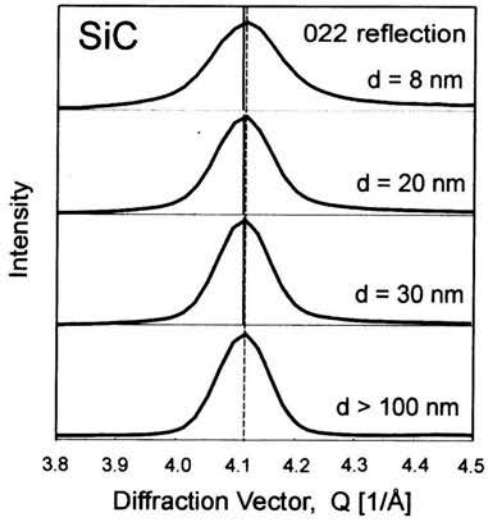

FIGURE 22. (220) reflections measured for SiC nanocrystals of different grain size.

TABLE 1. Relative shift of the position of the Bragg reflections caused by the presence of strain in the surface shell calculated for spherical SiC nanocrystals (6 and 12 nm in diameter). Surface shell thickness, $s_0 = 0.7$ nm; compressive surface strain $\Delta a/a_0 = -5\%$, (cf. Fig. 21).

d [nm]	hkl	2Θ	$\Delta 2\Theta^*$ [°C]	Δd^* [Å]	Δalp^* [Å]
$\lambda = 0.12$ Å (synchrotron)					
6 nm	111	2.736	0.013	−0.0130	−0.022
12 nm			0.008	−0.0027	−0.020
6 nm	246	11.839	0.058	−0.0130	−0.022
12 nm			0.039	−0.0027	−0.020
$\lambda = 0.7$ Å (MoKα)					
6 nm	111	16.087	0.077	−0.0130	−0.022
12 nm			0.052	−0.0027	−0.020
6 nm	246	73.969	0.425	−0.0130	−0.022
12 nm			0.281	−0.0027	−0.020
$\lambda = 1.54$ Å (CuKα)					
6 nm	111	35.682	0.177	−0.0130	−0.022
12 nm			0.118	−0.0027	−0.020
6 nm	246	−**	–	–	–
12 nm			–	–	–

*) $\Delta(2\Theta)$ is the change of the angular position (2Θ) of the Bragg reflection due to a presence of strain in the surface shell, Δd and Δalp are the corresponding changes of the interplanar d-spacings (calculated from the shifts of the Bragg reflections) and the alp values (calculated from the d-values according to the quadratic equation: $1/d^2 = (h^2 + k^2 + l^2)/(alp)^2$), respectively.

**) this reflection is beyond the Q-range of CuKα radiation ($Q_{max} = 4\pi \sin 90°/(1.54\,\text{Å}) = 8.16\,\text{Å}^{-1}$).

wavelength radiation needs to be applied. To determine precisely the position of a reflection (and, thus, the relative shifts of the reflections necessary for the *alp*-Q plots) a possibly long wavelength is needed: for the Bragg line (111), 0.12 Å radiation, and a 12 nm strained grain the shift of the angular position 2Θ of the reflection is only 0.008°, but increases 15 times (to 0.118°) when CuKα radiation is applied. However, with CuKα radiation the available range of the diffraction vector Q is less than 8 Å^{-1} (and practically even much less due to the technical limitations of the diffractometer itself), Table 1. Therefore, every design of a specific diffraction experiment is a compromise between the range of the available diffraction vector Q and the precision of the measurements of the peak positions. Angular dispersive diffraction measurements are made in a step-scan mode. The resolution of the measurements is determined by the divergence of the incident beam and the geometry of the detection system. The length of the scan step should be adequate to the actual limits of the particular experimental setting. When designing a diffraction experiment one has to evaluate the resolution required for the detection of the expected diffraction effects. In our case (the analysis of the *alp*-Q relations) we have to focus either on recording in a wide Q-range or on a precise measurement of the positions of relatively low Q-value reflections. We performed a number of different experiments using synchrotron sources making different compromises: to measure at a very large Q-range (up to 25-30 Å^{-1}) with a moderate resolution we used the Station ID11 at ESRF and Station BW5 at HASYLAB (wavelength 0.1-0.2 Å); to get a very good resolution we used the wavelength of 0.5-0.7 Å at SNBL Station at ESRF ($Q_{\max} = 10 - 15$ Å^{-1}). In addition to the advantage of the short wavelength radiation not available with sealed X-ray tubes, the powder diffraction instruments installed at synchrotron sources have usually much better angular resolution that those available in conventional laboratories.

5.1. Effect of the model parameters on *alp*-Q relation

We performed a systematic theoretical study of diffraction by nanocrystalline materials using models with different thickness of the surface layer, various magnitudes of the surface strain, and diverse gradients of the strain in the shell. The dependence of the *alp* on Q for SiC nanocrystals with the same strain of +5% and the surface shell thickness of 0.7 nm but different grain size is shown in Fig. 23. For a reference, the graphs contain also the *alp*-Q results for the corresponding models with a fully relaxed (unstrained) lattice.

The calculated deviations of *alp* from the core value of a_0 for strained grains are much larger than for those with the relaxed lattice. The difference between the *alp* and a_0 values increases with a decrease in the grain size, reaching as much as 1.7% of the lattice parameter of the relaxed SiC crystal for the 3 nm particle. These results are not surprising: for a 0.7 nm thick shell the strained fraction of the grain contains from 85 percent (for the smallest, 3 nm in diameter) to 31 percent (for the largest, 12 nm) of all the atoms in the particle. The results shown in Fig. 23 illustrate the consequences of using a standard powder diffraction technique combined with commonly applied radiation sources. The widely used Cu Kα X-ray radiation source allows for a collection of diffraction data in the Q-range up to only 5-7 Å^{-1}. For strained particles shown in Fig. 23 a routine elaboration of such data using the

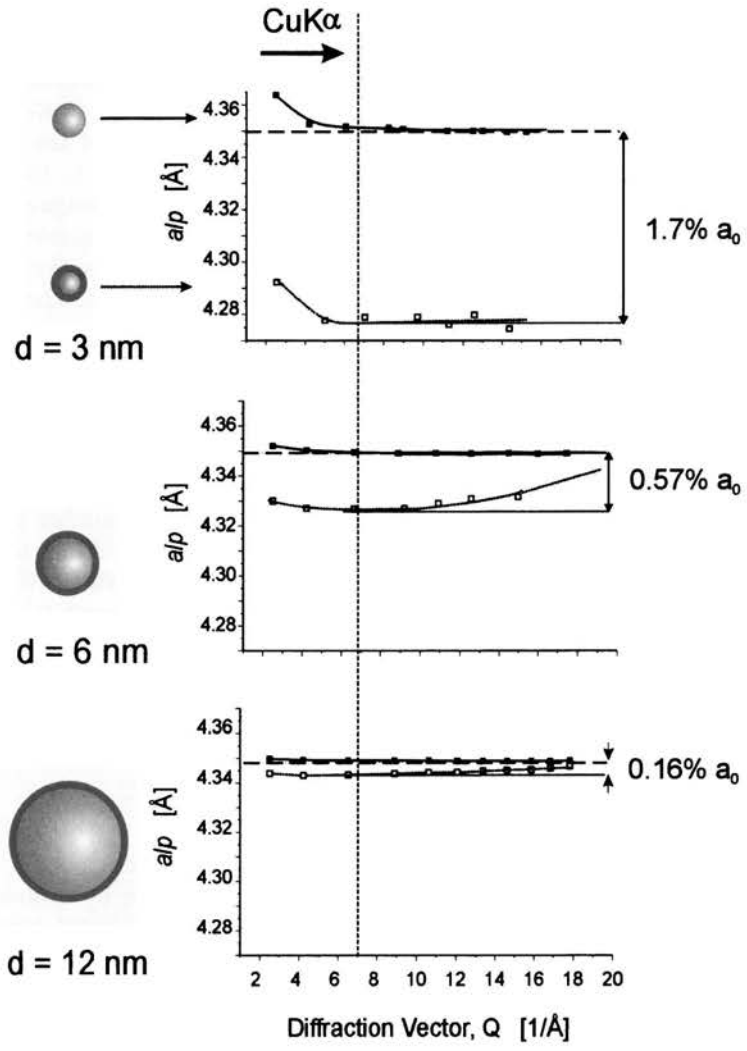

FIGURE 23. *Alp* values calculated theoretically for nanocrystalline cubic SiC of different grain size. $a_0 = 4.349$ Å; $\Delta a/a_0 = -5\%$, $s_0 = 0.7$ nm.

Rietveld program would yield the lattice parameters differing from a_0 of the relaxed lattice from 0.16 up to about 1.7% (Fig. 23).

A single *alp* value determined from a diffraction pattern has no specific meaning: only a set of *alp* values in a wider Q range can provide a meaningful information about the structure of the nanocrystal. The *alp* values at sufficiently high Q-values correspond to the lattice parameters of the core of the particle, the relaxed lattice. The experimentally determined dependence of *alp* on Q combined with numerical simulations can provide a meaningful information about the structure of the sur-

face shell of the nanocrystal. Examples of *alp-Q* data determined from theoretical diffraction patterns calculated for different models of SiC nanocrystals are shown in Figs. 24-26. The sensitivity of the *alp* values on the parameters of the model is

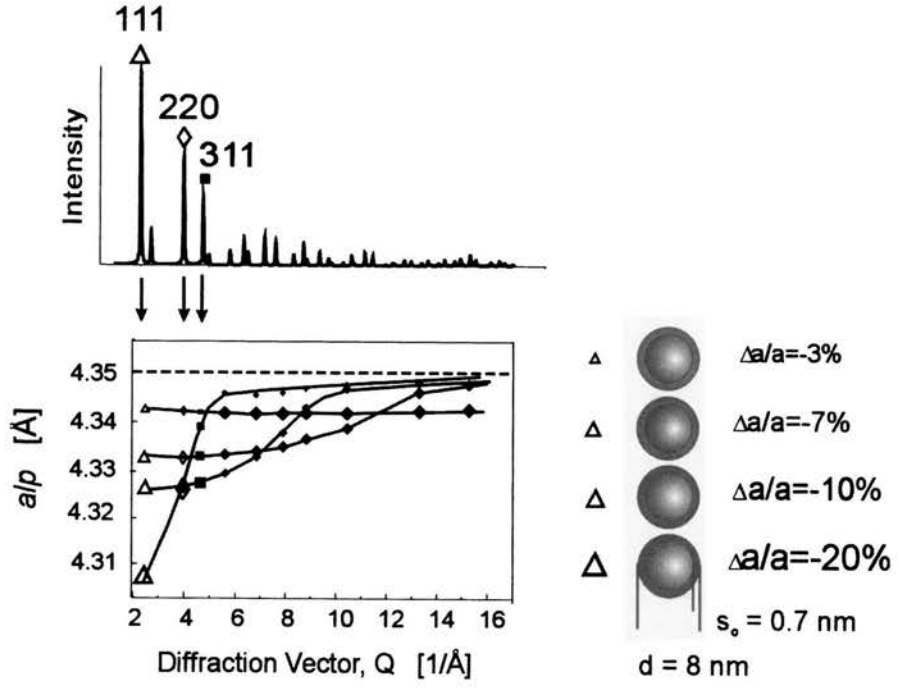

FIGURE 24. *Alp-Q* plots calculated theoretically for spherical 8 nm diameter SiC nanocrystals for different values of the compressive stress in the surface shell. $s_0 = 0.7$ nm.

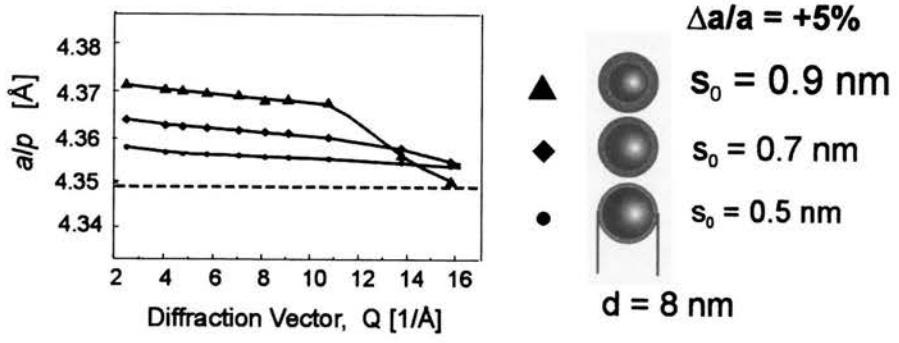

FIGURE 25. *Alp-Q* plots calculated theoretically for spherical 8 nm diameter SiC nanocrystals for different thickness of the surface shell. $\Delta a/a_0 = +5\%$.

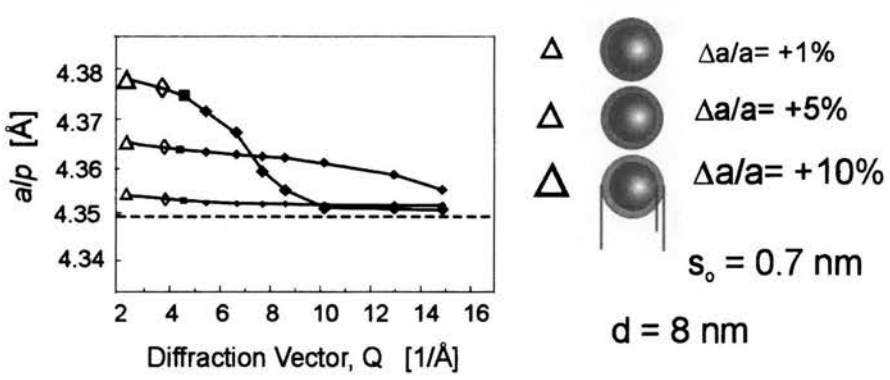

FIGURE 26. *Alp-Q* plots calculated theoretically for spherical 8 nm diameter SiC nanocrystals for different strain values in the surface shell.

quite high: differences as small as 1% in the lattice strain and 0.1 nm in the thickness s_0 of the surface shell are clearly visible (Figs. 24-26). Athough in all models the lattice parameter of the grain core is the same ($a_0 = 4.349$ Å – relaxed lattice) the *alp* values practically never reach a_0 except for greater Q's and larger surface strains. This shows that conventional diffraction experiments (low intensity laboratory sources, CuKα or MoKα, maximum Q range of 7 and 15 Å^{-1}, respectively, elucidation of the common lattice parameters from the entire diffraction diagram) do not allow for a unique interpretation of the lattice parameters calculated from the Bragg reflections.

In our theoretical calculations both the strain in the surface shell and the lattice parameters of the grain core are variable parameters of the core-shell model. For that reason the interpretation of the *alp-Q* results needs to be done with caution. The plots presented in this paper have well defined shapes which show a dependence between the lattice parameters of the grain core and the strain in the surface shell. However, our analysis is performed as if the atomic lattice of the materials consisted of some atomic planes spaced by a well defined distance. In reality the lattice of the nanograins does not form planes but bent surfaces (Fig. 18), so the use of the Bragg relations in the calculations of the *alp* values yields some average spacings between the deformed planes and not the real interplanar distances. Nevertheless, powder diffraction data combined with our *alp* methodology (based on geometrical factors alone) can provide quite realistic but still approximate model of the core-shell structure of the nanocrystal. Based on our analysis we conclude, that the correct values of the lattice parameters of the grain cores can be determined from the diffraction experiments performed in a wide range of the Q vector. To determine the specific positions of atoms in the surface shell an analysis of the relative intensities of the Bragg-like reflections is necessary. Currently we are investigating an alternate approach to determination of interatomic distances in these materials using neutron diffraction and the so-called "real-space Rietveld refinement" technique [39, 40].

5.2. Application of the concept of *alp* to the evaluation of experimental diffraction data of nanopowders

We applied our methodology for evaluation of the experimental diffraction data of different nanocrystals. The powder diffraction patterns in the range up to $Q = 20\,\text{Å}^{-1}$ were obtained using a short wavelength synchrotron radiation sources (at BW5 Station at HASYLAB, and ID 11 and SNBL powder diffractometers at ESRF). At the present stage of our studies we can claim a qualitative agreement between the *alp*-Q plots determined from the experimental powder diffraction data of nanocrystalline SiC, GaN and diamond, and our theoretical calculations. For example, we deduced that a tensile strain exists in the surface shell of nanocrystalline SiC (compare Figs. 15 and 26). Similiar strain is present in diamond nanoparticles. Opposite in sign, compressive strain at the surface is present in a much softer material, nanocrystalline GaN (Fig. 27).

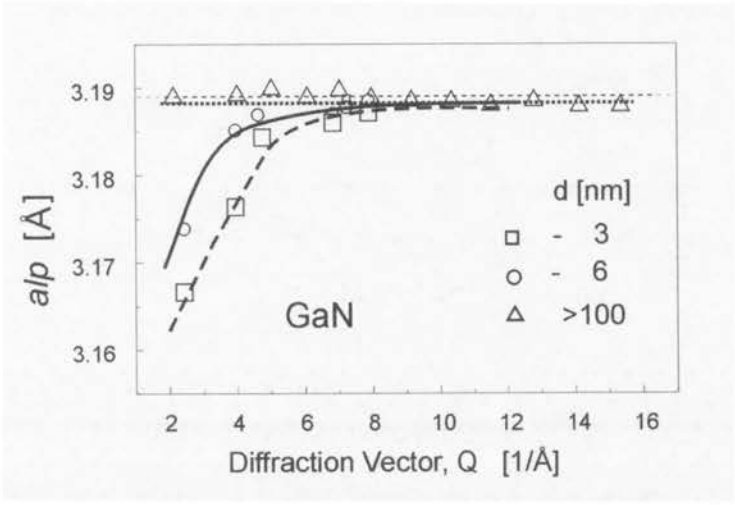

FIGURE 27. *Alp*-Q plots obtained experimentally for GaN nanocrystals.

The surface of a nanoparticle is in a metastable state and, thus, is strongly dependent on its surrounding. The surface exposed to a gas, liquid or solid medium can adsorb foreign atoms or even undergo a chemical reaction. When that happens the properties of the surface change accordingly, what is widely used in catalytic reactions and sorption processes. Interaction of the surface with foreign atoms must affect the atomic structure of the surface. We have examined this problem in a series of experiments performed for nanocrystalline powders of diamond and SiC. The powders were annealed at elevated temperature under vacuum used as components of ceramic composites. Representative plots of the *alp* values vs. the Q vector are given in Figs. 28-30.

Desorption of foreign atoms from the powders apparently leads to a considerable contraction of the surface shell (relative to the raw material, aged in the air) as indicated by the reduction (in the *alp* values) in the low Q range (Fig. 28). Similiar

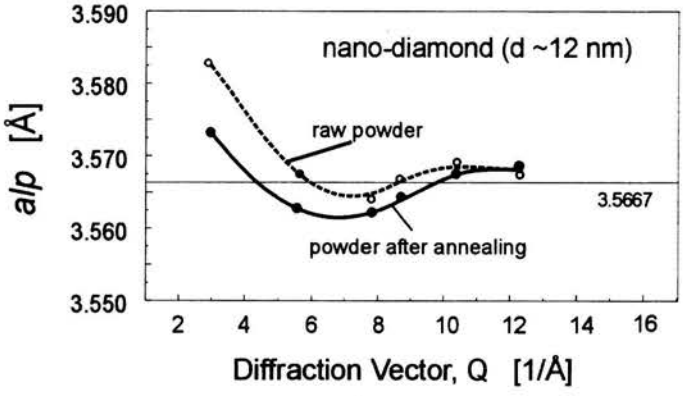

FIGURE 28. *Alp-Q* plots obtained experimentally for diamond nanocrystals aged in the air (dotted line) and annealed in vacuum at 400 °C for 4 hrs (solid line).

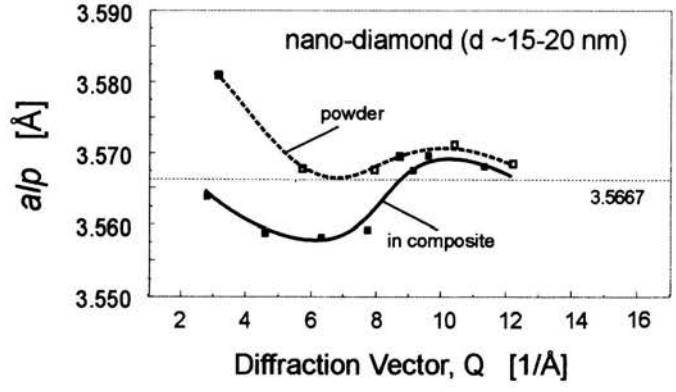

FIGURE 29. *Alp-Q* plots obtained experimentally for raw diamond nanocrystalline powder (dotted line) and that embedded in the diamond-SiC nanocomposite (solid line).

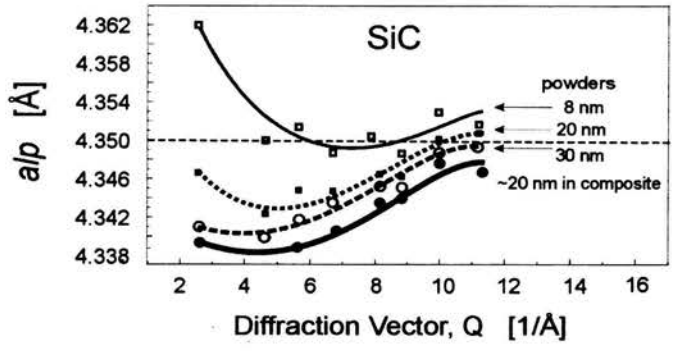

FIGURE 30. *Alp-Q* plots obtained experimentally for SiC nanocrystals with a different grain size and for a 20 nm diameter nanocrystalline SiC embedded in the diamond-SiC nanocomposite.

effect is observed when the environment of the grains changes to a dense matrix of the composite (Figs. 29 and 30).

The experiments perfomed on differently processed nanocrystalline SiC and diamond show very clearly that the structure of the surface shell in nanocrystals depends strongly on the amount and type of foreign atoms adsorbed on the grain surface. This observation is not surprising: our DTA and mass spectroscopy measurements showed that during annealing of raw powders of SiC and diamond in a vacuum and/or inert gas atmosphere the materials lose up to 10% of their initial weight. Apparent changes of the grain surface environment during densification and sintering into dense ceramics leads to changes in the atomic structure of the surface shell (Figs. 29 and 30).

In this work we did not attempt to achieve a quantitative evaluation of the observed changes of *alp* values with Q; additional measurements of specific physical properties of our materials are necessary to examine what kind of changes occur at the surface and how much they affect the structure of the grain core. The *alp* concept provides a sensitive tool for investigation of the structural features of very small, nanosized crystallites. From our preliminary calculations based on the models of nanocrystals with different surface strain and thickness we conclude that annealing of diamond powders leads to a significant reduction in the strain present in the surface shell without much change to the structure of the grain core. This is indicated by the strongest changes of the *alp* occuring in the low Q range (which is very sensitive to the structure of the surface shell) and a convergence of the *alp*s of raw and processed powders at larger Q values (Fig. 28). The *alp*-Q dependence for nanocrystals of SiC in the form of a powder and in the composite with diamond show very similar shapes but the *alp* values measured for the composite environment are lower than those for the powder even at the wide Q range (Figs. 29 and 30).

The results of our experimental work presented in this paper are only preliminary. A more definite description of the structure of nanosize particles requires both additional examination of the physical properties and structure of the materials (using techniques sensitive to the local atomic configuration, like Raman or IR spectroscopy) and more extensive modelling efforts that would include different strain fields both in terms of strength and distribution in the surface and core of the grain. That includes the non-monotonic nature of the *alp*-Q relations observed in Figs. 28-30 which may be due to the anisotropic shape of the real grains and/or the grain size distribution.

6. Summary and conclusions

The methodology of the structural analysis of micrometer-size polycrystals is well established and approximations made for the description of the structure of such materials and for the analysis of their diffraction data provide satisfactory results. However, the conventional tools developed for elaboration of powder diffraction data are not directly applicable to nanocrystals:

- Nanoparticles have a complex structure that resembles rather a two-phase than a uniform, one-phase material. Therefore the definitions and parameters used for characterization of the atomic structure of simple, crystallographically

uniform phases are insufficient for the description of the complex structure of nanocrystals;

- Conventional powder diffraction techniques and appropriate methods of their elaboration have been developed for materials showing a perfect, three-dimensional, periodic order in an infinite crystal lattice. A nanocrystal is a finite in size crystal where the effect of boundaries cannot be ignored. For very small, several nm in diameter crystallites the number of atoms at the surface can exceed the number of atoms in the grain core. The structural and other properties of the surface atoms can dominate over the effects imposed by the bulk atoms. This effect is clearly observed in our diffraction experiments.

This work is dedicated to the methodology of elaboration of powder diffraction data of nanocrystals, not to the determination of the atomic structure of some specific materials. We have shown the limitations of a conventional structural analysis approach and proposed a new method of evaluation of diffraction data of nanosize polycrystalline materials. We have demonstrated a qualitative agreement between the experimental results and those obtained by numerical modelling using our *alp* concept methodology. A more complete evaluation of powder diffraction data of specific nanocrystalline materials requires a wider spectrum of structural models as well as accounting for the shape and size distribution of nanocrystals in real materials. The work on these issues is in progress.

While the application of conventional methods of structural analysis to nanomaterials has its fundamental limitations, a new field of the structural analysis opens up. A manageable number of atoms in individual crystallites make it feasible to build a complete model of the particles and calculate the diffraction patterns of such materials. We used this possibility to model the atomic structure of different nanocrystals and to calculate the corresponding diffraction effects without any simplifications to the theory of diffraction. Our analysis of the diffraction experiments presented in this work concerned only the geometrical parameters describing the ordering of atoms in nanocrystals. We did not discuss any specific atomic structures, in particular the occupancy of the lattice positions by specific atoms or the effect of the lattice vibrations. Such approach would require a quantitative analysis of the intensity profiles of the scattering beams what is outside the scope of the present work.

In this paper we have shown the limits of applicability of well-established methods of structural analysis of materials by the diffraction techniques. When it comes to nanomaterials there are obviously limitations of other commonly applied techniques and procedures used in determination of different physical properties of materials. A development of new experimental and theoretical tools for investigation of unique properties of nanocrystals is a challenge and a must.

Nanocrystals are often referred to in the literature as two-phase materials. This is a useful concept although it defies the basic definitions of a crystallographic phase. The problem with such approach is, that the two phases form essentially a composite crystal with interfering, unseparable diffraction properties. The core-shell model of a nanocrystal applied in this work is, in fact, a kind of a two-phase system that exhibits unique diffraction features. Apparently this situation requires a new approach to the structural analysis of such systems. One should realize that

complex atomic structures cannot be well described using only basic, fundamental definitions. The limitations of the currently used definitions become obvious in the rapidly developing field of nanomaterials.

II. High-pressure studies of nanocrystalline materials

7. Introduction

In situ high pressure (h-p) powder diffraction experiments are widely used to examine the strength of interatomic interactions through determination of the material's compressibility [41, 42]. As shown in Fig. 31, the interatomic potential of a two-atom system, ϕ, depends on the distance between the atoms and has a minimum determining the equilibrium interatomic distance r_0. Application of an external force along the interatomic bond leads to a change of the distance r according to the relation $F = \delta\phi/\delta r$ (Fig. 31a). Interpretation of changes of interatomic distances in a solid is difficult due to a large number of interacting atoms and short- and long-range forces. The potential describing the equilibrium state of such a system is a complex, three dimensional, usually anisotropic function. In general, the effect of force (stress) on interatomic distances can be analyzed for any array of atoms. Such analysis would be very complex therefore, for practical reasons, the effect of stress is being investigated through measurements of the overall properties of bulk material. This can be done experimentally by application of a homogenous stress (hydrostatic pressure) what can be accomplished using a fluid medium. Thus, instead of considering changes of individual interatomic distances compression of the entire material is being analyzed.

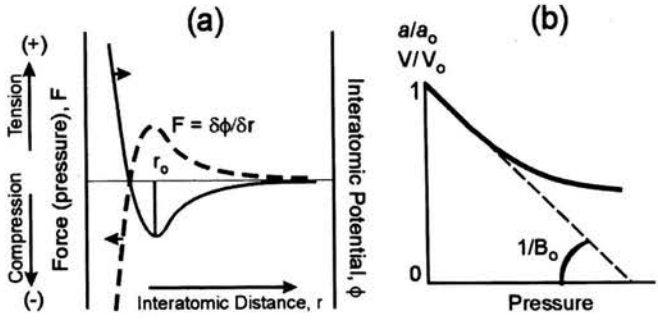

FIGURE 31. Compression in materials: (a) interatomic potential and related interatomic force, (b) compression curve.

Behavior of solids under pressure is conventionally characterized by the bulk modulus B_0 defined as the relative change of the volume of the sample per unit change of the applied external (hydrostatic) pressure. In the elastic region of the compression curve the relative change of the volume, $\delta V/V$, is proportional to the change of the applied pressure δP, Eq. (7.1):

$$\frac{\delta V}{V} = -\frac{\delta P}{B_0}, \tag{7.1}$$

where B_0 is Bulk Modulus. Beyond the elastic region, a further increase in pressure leads to a decreasing compression of the material (Fig. 31b). Several equations of state describing this nonlinear behaviour, e.g. Murnaghan, Eq. (7.2), or Birch first order equation of state, Eq. (7.3), were proposed [41, 42]:

$$P = \frac{B_0}{B_0'}\left[\left(\frac{V_0}{V}\right)^{B_0'} - 1\right], \tag{7.2}$$

$$P = \frac{3}{2}B_0\left[\left(\frac{V_0}{V}\right)^{7/9} - \left(\frac{V_0}{V}\right)^{5/9}\right]\left\{1 + \frac{3}{4}(B_0' - 4)\left[\left(\frac{V_0}{V}\right)^{2/3} - 1\right]\right\}. \tag{7.3}$$

In this work, based on the analysis of experimentally determined changes of the lattice parameters, we examine the structural changes in nanocrystalline powders. The analysis concerns both the compression of the entire crystal lattice (formation of *macro*-strains) and generation of *micro*-strains in the structure.

Elastic properties of crystalline materials are described based on the bulk modulus that applies to any form and shape of a crystalline material: single crystals, polycrystals, crystalline layers, etc. From this point of view, neither particular techniques of high-pressure studies, nor any special methods of diffraction data elaboration are required in the investigation of nanocrystalline materials. However, as will be shown below, interpretation of the experimental diffraction data of nanocrystals collected under external stresses (high pressure) is very laborious and requires an application of some non-standard experimental and theoretical methodologies. This is due to, (i), a presence of internal pressure in as-grown nanograins (e.g. [43]-[46]) and, (ii), non-uniform atomic structure of nanocrystals resembling rather a two-phase than a one-phase material. Additionally, a description of the atomic structure of nanocrystals by the lattice parameters is questionable: the values of the lattice parameters determined from the Bragg equation are not unique [47, 48].

In this part of the lectures we will discuss specific problems of conducting and elaborating the results of high-pressure diffraction experiments on nanocrystals: (i), compression of nanocrystalline powders without a pressure medium, i.e. under the so-called isostatic pressure conditions (we call this process "densification") and, (ii), compression of nanopowders under hydrostatic pressure conditions, [49]-[53]. We will discuss the effects of application of external stresses to nanopowders applying a core-shell model of nanocrystals [47, 48] for the interpretation of our h-p diffraction experiments on nanocrystalline SiC and GaN powders.

8. Specific properties of nanocrystals

Nanomaterial is a solid with at least one characteristic dimension on the order of nanometers [54]-[58]. The atomic structure of such materials can be amorphous or crystalline. They can have any shape, and the characteristic nano-size can extend in one-, two-, or three-dimensions. Such small size adds an extra "degree of freedom" to the materials behaviour in the sense that a change of the particle size into the

nanoscale range changes its structural and physical properties even if changes of its lattice parameters are not detected in conventional experimental measurements. This in particular applies to the structural properties determined using powder diffraction methods [59]-[61]. With a decrease in the size of the powder grains the specific surface area increases. In nanocrystals with several to a few tens of nanometers in size the specific surface is on the order of tens and even hundreds of m^2 per gram. For instance, a 5 μm copper powder has the specific surface area of 0.134 m^2/g, while a 5 nm grain diameter powder – 134 m^2/g. The surface atoms are always in a higher energy state than those in the interior of the grains and, thus, dispersed materials always show a tendency to reduce their surface. This obvious tendency of nanocrystals to reduce the free surface leads to a rearrangement of the surface atoms and to some reconstruction of the crystal lattice [43]-[46], [62]-[68]. (The reconstruction of the surface that occurs in polycrystals is different than that which takes place on a flat extended surface of a single crystal terminated by well defined atomic planes. The surface of a small particle is combined of a variety of different atomic planes, its structure is not unique, and the interatomic spacings at the surface are not well known). Due to the small size, nanocrystals always have strongly curved surfaces. The direct consequence of the extreme surface curvature is a topological instability of nanoparticles. To lower the total surface energy each isolated particle tends to convert the high-energy planes into those having smaller excess energies. In real materials only local equilibria between the actual outer atomic planes exist, i.e. each nanoparticle is in a metastable state. The general specifics of nanocrystalline materials described above are independent on the actual atomic structure of a given particle.

Nanocrystals exist as loose powders as well as solids (compacts or composites), both types of phases constituting a metastable state of the matter. The instability is due to an excess free surface energy in powders, and excess grain boundary energy in bulk solids. The atoms in the grain boundaries have higher energy than those in the interior of the individual grains. Since nanocrystals have very high density of grain boundaries, nanomaterials exhibit a range of unique physical properties qualitatively different from those of their corresponding "ordinary size" materials. Nanocrystals show size-dependent properties, e.g., enhanced diffusivity and strength/hardness, reduced density, higher electrical resistivity, increased specific heat, enhanced thermal expansion coefficient, lower thermal conductivity and superior soft magnetic properties [54]-[57], [69]-[77]. The origin of the unique properties of nanocrystals is not well understood. In some cases the observed new properties are interpreted as having the same origin as "ordinary" materials, but their specific physical behaviour is enhanced due to the very small size. Many new properties of nanocrystals are quite unique, some stemming from very strong interactions between the interfaces that are due to the quantum effects related to the very small size of the particles, etc. (e.g. [78]).

Information on different physical properties must be consistent with the physical model of the material and explain its specific properties: structural, mechanical (elastoplastic), electrical, optical, etc. Based on such a model one should be able to predict (calculate) the behaviour of the material under particular conditions. Research on a physical model of nanocrystals is at an early stage of development. Although a lot of information on the unique properties of different classes of nano-

materials is available in the literature, relatively little is known about the origin of those properties. A model of the atomic structure of very small crystals, nanocrystals with a few to a few tens of a nanometer in diameter, to which the measured specific properties could be referred to, is badly needed. A model of nanocrystal where a grain core is surrounded by a surface shell with a different structure has been discussed in the literature, but the concept has never been verified experimentally. Recently we examined theoretically a core-shell model where the core has a well-defined crystallographic phase while the surface shell has the atomic structure similar to and correlated with that of the grain core but modified by the strains present at the surface. We verified this model based on our experimental powder diffraction data. We showed that diffraction data obtained for a very large diffraction vector range are sensitive enough to detect even small differences between the interatomic distances in the grain's core and shell [47, 48]. According to the core-shell model (which is essentially a two-phase model), the properties of nanocrystals should be referred to the two phases of the material and not to one, uniform structure characteristic for bulk crystals. This should apply to any physical property of a nanomaterial, in particular to overall elastic properties of nanocrystals. Here we focus on the elastic properties of nanocrystals of SiC and GaN examined with *in situ* high-pressure diffraction techniques.

9. Should one expect an effect of size on the properties of polycrystalline materials under pressure?

The atoms present at the very surface of any material have fewer bonds and, thus, different surrounding than those in the bulk. In addition, the atoms just underneath the surface have their next nearest neighbor bonds different than those in the grain core. To compensate for different surrounding of atoms (a difference in the interatomic potential) in the interior and the outer layer the surface of the solid, while maintaining the total number of atoms in the material, can undergo a modification by elastic deformations or restructuring. A presence of any kind of surface stress always affects the properties of the material under pressure. (These properties are not described by the compressibility modulus which characterizes the bulk properties only.) The effect of surface stresses can be significant for nanocrystalline powders with very large specific surface area. That problem has not been a subject of serious studies yet. However, a number of publications indicate that such fundamental materials properties like lattice parameters and phase transition points are dependent on the grain size of polycrystals [78]-[83].

Following the general theory of surface tension it is often concluded that the surface atoms tend to lower the accumulated surface energy γ by contraction [43]-[45]. The surface stress f can be either positive or negative (tensile or compressive surface stress, respectively). For high symmetry solid surfaces the stress, which acts tangentially to the surface, can be taken as a scalar, $f = \gamma + d\gamma/de$, where de is a change in the elastic strain in the surface. When the elastic and plastic terms are accounted for the term $d\gamma/de$ can be negative and formation of dislocations and elastic buckling of the surface can occur. This could lead to hardening of the free surface and grain boundaries in powders and dense (solid) nanocrystals.

In a small, single-component spherical solid crystal with an isotropic surface stress f, the surface exerts a hydrostatic pressure ΔP that is added to the external pressure to balance the internal pressure in the solid. The Laplace pressure for such particles can be expressed as $\Delta P = 2f/r$. This applies both to spherical as well as to facetted crystals of any shape. A presence of internal pressure leads to a compression of the interior of the particle (the grain core). Compression of the core should be detectable through a measurement of the lattice parameters of the material: $\Delta P = -(\Delta a/a)3B_0$, where B_0 is the bulk modulus. A dependence of compressibility on the size of nanocrystals has indeed been reported in the literature with a suggestion that this effect is due to a presence of internal pressure caused by the surface tension [84]-[88].

The specific relations involving surface stresses discussed above can be applied to larger particles where the thickness of the surface layer is very small relative to the dimensions of the entire particle. In a real crystallite the surface energy and/or stress is not confined to the very surface but extends over a number of atoms across the surface layer (shell). Thus, both the grain core and the surface shell should have different properties, in particular different bulk modulus B_0. As a consequence, the concept of the surface tension and its relation to the internal pressure defined in the Laplace formula cannot be applied directly to nanoparticles.

In this paper we analyze diffraction data of nanocrystalline powders obtained under high stresses based on two alternate assumptions: (i), the crystals are a uniform, unambiguous structure, or, (ii), the grains constitute a two phase, core-shell system. The basic question which we will try to answer is how far the interpretation of the diffraction patterns measured experimentally under pressure could be related to the regular (determined for large grains) compressibility data of the material.

10. Powder diffraction under high pressure

High-pressure diffraction experiments require special equipment and procedures [41, 42]. Application of high pressure to a sample requires special constructions where a certain amount of the sample is tightly closed in a volume to which an external stress is applied. Due to technical limitations of the materials exposed to extreme loads, the volume in which the pressure can be generated strongly decreases with an increase in the maximum pressure available in the apparatus. The equipment capable to withstand a pressure of tens of GPa can accommodate samples up to about 0.001 mm^3 in size. The commonly used sample holder is the Diamond Anvil Cell (DAC), Fig. 32. In DAC assembly two diamond single crystals, a few millimeter in diameter each, are used as the opposite anvils. A 0.1-0.2 mm thick metal gasket with a 0.1-0.2 mm diameter hole in the center is placed between the anvils. The sample is placed in the hole and sealed/confined between the diamonds. By increasing the external load the gasket is squeezed and the sample volume decreases what leads to an increase of the pressure inside the sample volume. Presses of different construction are being used [41].

In the most common configuration of a powder diffraction experiment the diffracted intensity is measured by a detector which scans over the diffraction angle 2Θ. Because the diamonds that generate pressure have to be supported by a strong,

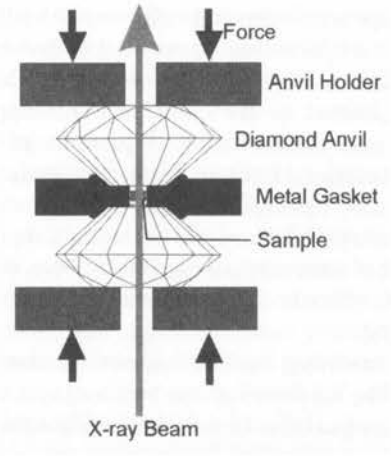

FIGURE 32. Scheme of the Diamond Anvil Cell (DAC) assembly.

massive construction, the access to the sample area is limited to a relatively small angle about the DAC axis. For that reason the most suitable technique for those measurements is the energy dispersive geometry, where the diffraction pattern is collected as a function of the energy of the beam diffracted at the (fixed) detector angle Θ_0 (Fig. 33a) [42]. For such geometry the Bragg equation written as a function of energy is used:

$$2d_{hkl} \sin \Theta_0 = \lambda_{hkl} = \frac{h\,c}{E_{hkl}} = \frac{12.398}{E_{hkl}}, \tag{10.1}$$

where h is the Planck's constant, c – velocity of light, d_{hkl} – the interplanar spacing, and E_{hkl} – the energy of photons (in keV) obeying the Bragg equation for a

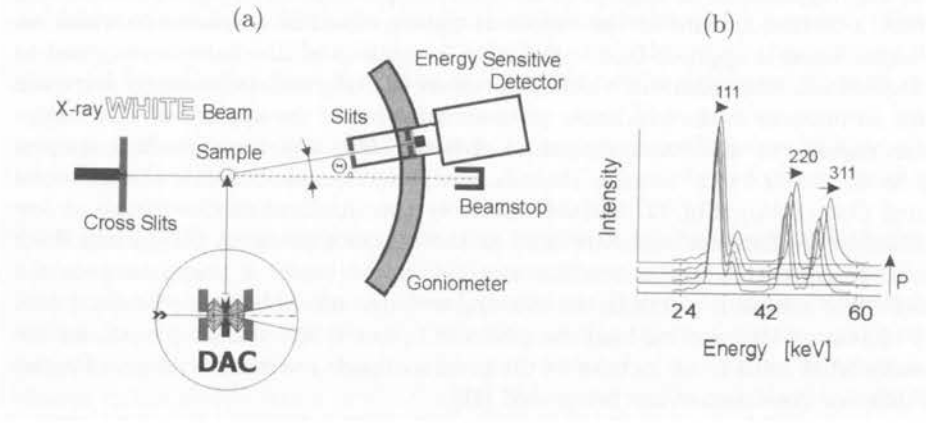

FIGURE 33. Powder diffraction under high pressure in the energy dispersive geometry: (a) configuration of *in situ* experiments, (b) typical powder diffraction patterns obtained under different pressures.

given d_{hkl}. The experimentally accessible range of the measured d_{hkl} values depends on the detector angle Θ_0 (Fig. 34). This condition is similar to selection of the wavelength of the incident beam in the angular dispersive geometry of the diffraction experiments.

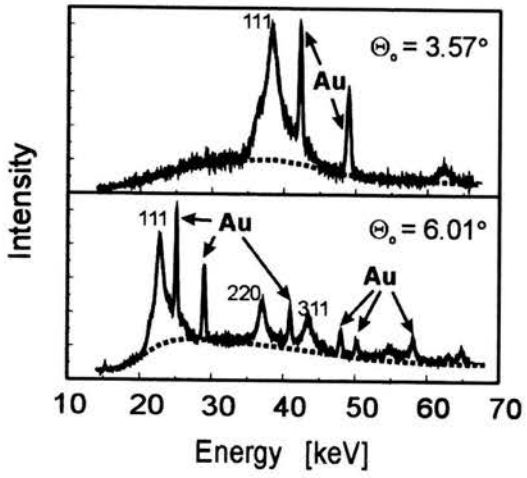

FIGURE 34. Diffraction patterns of a cubic GaN sample (4 nm in diameter) obtained at different detector angles Θ_0.

For polycrystalline materials it is convenient to determine the pressure inside the sample volume using internal pressure markers. The marker is a relatively soft material (small bulk modulus) with a known compressibility. A very small amount of the marker is mixed with the sample and the signals from the sample and from the marker are registered simultaneously during the experiment. The pressure in the cell can be calculated from the measured positions of the Bragg reflections of the marker (Fig. 35). The diffraction patterns of the marker and of the examined sample should not overlap. Since the positions of the diffraction peaks of different materials change differently with pressure (see an overlap of NaCl and GaN reflections at different pressures, Fig. 35), a proper selection of the marker(s) should account for that effect.

Most of h-p diffraction experiments are being performed under hydrostatic pressure conditions. Such measurements can be done using solid or liquid pressure media like NaCl, vaseline, oils, alcohols, liquid argon, etc. [41]. Hydrostatic conditions are very difficult to accomplish in very small volumes like that in DAC where surface effects play an important role in generation of strains in the compressed sample material. This creates a particularly severe problem with brittle (non-plastic) polycrystalline materials where individual powder grains are in direct contact. Therefore, a very careful interpretation of the powder diffraction data collected with DAC is necessary, particularly at lower pressures when the contact area between the grains is very small what can lead to extreme stresses at the contact points. This problem diminishes with an increase of the sample volume where the amount of the hydrostatic

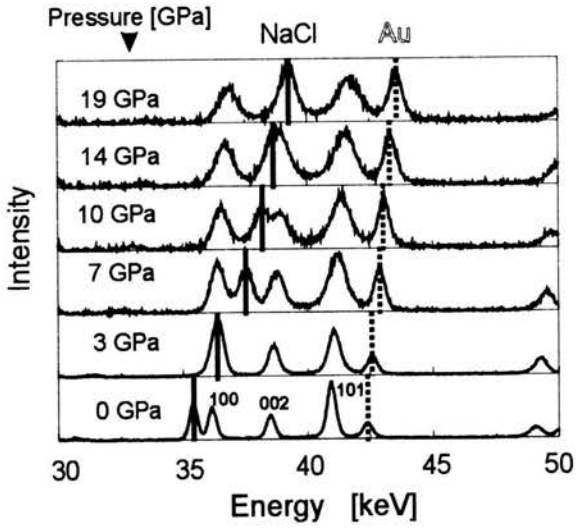

FIGURE 35. Diffraction patterns obtained under different pressures for 15 nm GaN powder with internal pressure markers (polycrystalline NaCl and Au).

pressure medium is much larger that that of the sample. To achieve such conditions in DAC the medium-to-sample volume ratio should be large, about 10 or more. Under these conditions, when the total volume of the sample is only $0.1 \times 0.1 \times 0.1\ \mathrm{mm}^3$, the amount of the sample material is so small that the diffraction signal may be too weak to be measurable with a reasonable accuracy (sufficient statistics). We performed our diffraction measurements in HASYLAB at DESY using a Diamond Anvil Cell (DAC – Station F3) capable of exerting the pressures up to 45 GPa (at room temperature), and the six anvil cubic press MAX80 (Station F2.1) accommodating larger sample volumes (0.5 cm^3) up to 8 GPa. Using the energy dispersive geometry, diffraction patterns with the diffraction vector values up to 3.5-4 $\mathrm{Å}^{-1}$ were measured with a reasonably good statistics. For higher Q-values good quality data could not be obtained due to a poor signal-to-background ratio. To obtain diffraction data for larger Q-values, measurements in DAC in the angular dispersive geometry using MoKα_1 radiation were performed.

We did a series of h-p diffraction experiments on nanocrystals in DAC using different pressure media and found that the results were dependent on the medium used: liquid Ar, mixture of alcohols, vaseline, silicon oil. The results presented in this work and obtained under hydrostatic pressure were done using silicon oil as the pressure medium. Other experiments discussed below were done without a pressure medium, i.e. under the so-called isostatic pressure conditions [48]-[51]. The measurements resemble the actual conditions of densification and sintering techniques, so such experimental configuration provides an insight into real and important technological processes.

11. Sensitivity of powder diffraction techniques to in-situ examination of strains in porous materials

A powder diffraction experiment provides information on the atomic structure of the material averaged over the entire volume penetrated by the incident beam [59]-[61]. That means, that the diffraction data contains information on the location of every single atom present in the material relative to all other atoms in the sample. The "only" problem is to extract this information from the diffraction data. A number of crystallographic programs are used to evaluate diffraction data. However, most of the programs are tailored to standard experiments and are used to obtain only basic information on the structure of the material. With respect to crystalline samples, such information provides a set of lattice parameters describing the shape and size of the unit cell (it is assumed that a unit cell represents the atomic structure of the entire crystal). More advanced elaboration methods extract information on the kind and positions of the atoms in the unit cell and their thermal motions. Diffraction is also sensitive to the lattice imperfections and disorder and, for very fine powders, depends on the size and shape of the grains.

In the diffraction experiments on powders under pressure, which are the subject of the present study, we intended to investigate *macro*- and *micro*-strains generated in the materials. Both kinds of strain have to be regarded as the sample parameters. The measure of *macro*-strains is the relative change of the lattice parameters per unit pressure interval, $(\Delta a/a)/\Delta P$. *Micro*-strain is a variation of the lattice parameters about the average value. As shown schematically in Fig. 36, a presence of *macro*-strains in a crystalline material shows in the diffraction pattern as a shift of the Bragg reflections from their reference positions (without changing the peak width, Fig. 36). A presence of *micro*-strains leads to broadening of the Bragg re-

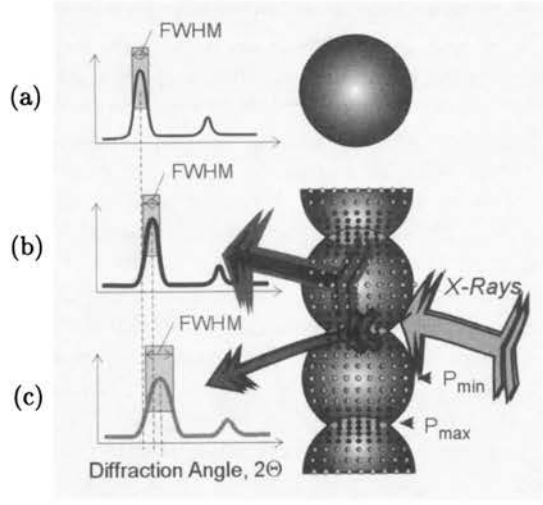

FIGURE 36. Effect of a presence of *macro*- and *micro*-strains on the position and width of the Bragg reflections: (a) relaxed lattice, (b) *macro*-strains, (c) *micro*-strains.

flections. When *micro*-strains cause a change of the average lattice parameter of the sample, the broadening is accompanied by a shift of the peak position as well (Fig. 36).

The basic elaboration of diffraction data includes determination of the positions and widths (usually as Full Width at Half Maximum - FWHM) of the Bragg reflections. To determine those values a function describing the shape of the experimentally measured Bragg reflections is needed. The diffraction peaks measured for materials with *micro*-strains have often asymmetric shapes and, thus, their positions and widths do not have unique values. Therefore the method of elaboration of the data should be carefully chosen and used consistently for all the experimental measurements. To determine the positions and widths of the Bragg reflections of our samples we used, as the standard procedure, a fit of the shape of the experimental peaks to the split-Pearson function. This function allows for an independent fit of the left and right shoulders of the peaks and can be conveniently applied for both symmetrical and asymmetrical lines. This way we were able to get rid of the strong scatter of the measured intensities (which is very critical in high pressure experiments due to very low net intensities of the peaks) and obtain reproducibly the intensity profiles of all reflections. The positions of the reflections were taken at the weighted center of intensity of the refined (fitted with the split-Pearson function) reflections.

12. Sources of non-uniform distribution of strains in polycrystals under external stresses

For our high pressure diffraction experiments made using DAC we use the term "pressure" which is calculated from the Bragg reflections of the internal standard (here: Au). Strictly speaking, the term "pressure" is fully adequate only if the applied external stress is transferred to the material through a hydrostatic medium. The ceramic powder placed in DAC without a pressure medium is a porous material, thus the term "pressure applied to the sample" is not fully adequate. The external load applied to the diamond anvils is transferred to the sample through the grains that are in direct contact with the anvils. These stresses are transferred to the grains underneath and, through the contact points between the grains, the external load is evenly distributed over the entire sample volume (Fig. 37). The local pressure is the actual stress transferred by the material (a chain of grains) to a given location divided by the surface area (cross-section) of that location, Fig. 37. Therefore, in the absence of a pressure medium, one should talk rather about distribution of stresses than about the pressure applied to the sample. In nanocrystalline materials with particles of only a few nm in diameter, the number of contact points is very large (in the volume of $1\,\mu m^3$ the number of particles 5 nm in diameter is approximately 10^8, the number of contact points about 10^9) and the distribution of stresses is quite homogenous; a nanocrystalline powder could serve as a pressure medium in applications of hydrostatic pressure to larger size objects. However, to simplify the description of the experiment we use the term "pressure" as determined with the pressure marker. The marker is not in a hydrostatic medium either, but its plasticity allows for a uniform distribution of stresses in the grains as confirmed by

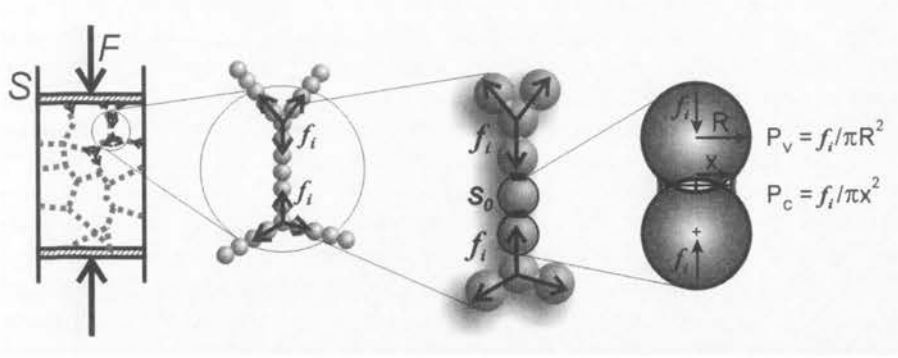

FIGURE 37. A model of distribution of microstrains during densification of a powder sample.

an absence of *micro*-strains in the material (no change in the width of the marker's reflections with a change in pressure indicating an accumulation of elastic energy in the form of *macro*-strains only). Our results on strains under isostatic pressure conditions refer to the essentially hydrostatic pressure conditions of the marker present in the sample.

Interpretation of an experiment performed under hydrostatic pressure is relatively simple and unambiguous. The results can be used to determine the bulk modulus or, with a more elaborate analysis, can provide the equation of state describing the lattice compression in the entire pressure range. (It is very difficult to assure completely hydrostatic pressure conditions, and some *micro*-strains are always present in materials subjected to external pressure.) An analysis of strains is never completely unambiguous. This is due to the fact that the energy transferred to the sample through the external load is accumulated not only as the elastic energy of the crystal lattice (manifesting itself as a change of the lattice parameters and its distribution about the average value) but in other forms of energy as well. Therefore, although the diffraction pattern contains complete information on *macro*- and *micro*-strains, a high-pressure experiment can reveal only the factors contributing to the characteristic diffraction pattern of the crystalline phases present in the sample. Information on *macro*-strains is obtained directly from the change of positions of the Bragg reflections (change of the lattice parameters). As the first approximation, information on *micro*-strains is extracted from the width of the Bragg reflections. *Micro*-strain is a localized state and changes from place-to-place in the sample volume, thus the information is averaged over the entire sample. Some forms of energy have no effect on Bragg reflections and cannot be measured quantitatively. For example, a presence of an amorphous phase is not associated with any characteristic Bragg reflections and its change upon pressure cannot be detected with diffraction methods. Therefore, there is always some uncertainty as to the completeness of information on strains in the materials derived from diffraction effects alone. Even for purely crystalline phases in the sample under pressure the interpretation of a diffraction experiment may be incorrect. Some sources of possible errors in the interpretation of *macro*- and *micro*-strains evaluated from powder diffraction patterns

obtained under external stresses are illustrated in Figs. 38 and 39. Figure 38 shows theoretical diffraction patterns calculated for 10 nm SiC grains with a cubic relaxed lattice and a similar pattern calculated for the same lattice but compressed under hydrostatic conditions (the lattice parameter was calculated from the bulk modulus of SiC). The calculations were done using the Debye functions [89, 90]. In both cases it was assumed that all grains have the same size and contain no microstrains. The shape of the calculated Bragg reflections is purely Gaussian and the widths of the corresponding peaks are identical for both pressures (Fig. 38). The third pattern in Fig. 38 is the sum of these two theoretical patterns. It simulates a sample being a mixture of equal amounts of relaxed and compressed SiC grains. (This situation may occur in samples where the external stress is not transferred to all parts of the sample volume, e.g. during high pressure densification of agglomerated powders with closed pores.) This composite pattern resembles that of a single-phase sample with the average lattice parameter corresponding to that under the pressure of 12.5 GPa. The apparent broadening of the composite peaks implies a presence of strong (in this case non-existing) *micro*-strains in the sample. In real practice the situation can be much more complex: the grain size is never uniform (leading to the Bragg reflections having shapes intermediate between Gaussian and Lorentzian), and they always contain some *micro*-strains. Also, the shape of the combined peak depends on the relative amount of the component, differently compressed fractions. In addition, a strong correlation between *macro*- and *micro*-strains, as determined from the diffraction data, is present (c.f. next sections).

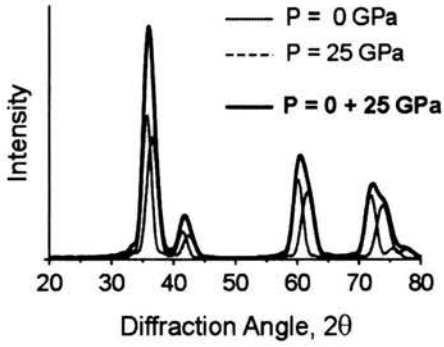

FIGURE 38. Diffraction patterns calculated for 10 nm SiC grains with a relaxed ($a = 4.35$ Å) and compressed ($a = 4.25$ Å at $P = 25$ GPa) lattice, dotted and dashed lines, respectively.

The results of an experiment that corresponds to the theoretical calculations shown in Fig. 38 is presented in Fig. 39. The samples were a mixture of microcrystalline or nanocrystalline diamond with 10 wt.% nanocrystalline SiC. Both powders belong to the class of super-hard, non-plastic materials, but have very different compressibilities. Stresses present in the samples were evaluated based on the lattice parameter a (the measure of *macro*-strains) and the width (the measure of *micro*-strains) calculated for the (111) Bragg reflection. The results for diamond are shown in Fig. 39a. A presence of SiC nanopowder has apparently no effect on

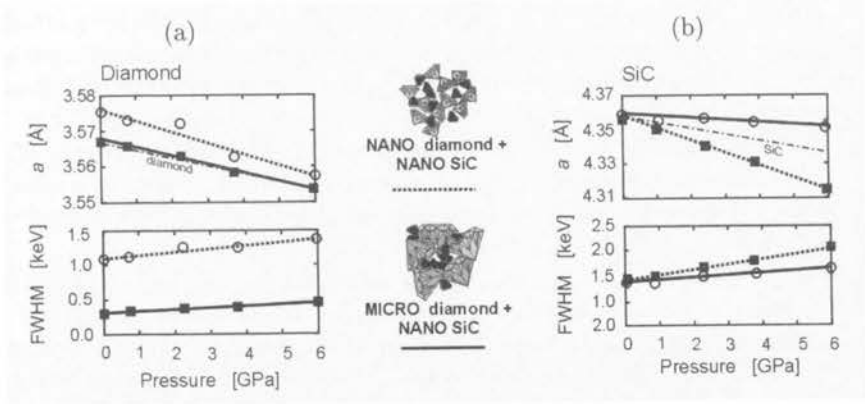

FIGURE 39. Experimentally measured change of the lattice parameter (top graph) and width (bottom graph) of the (111) Bragg reflection of a mixture of microcrystalline (dotted lines) and 10 nm nanocrystalline (solid lines) diamond powder with 10 wt.% of 10 nm nanocrystalline SiC. Dash-dotted lines – regular compression curves; (a) diamond, (b) SiC.

compression of diamond crystallites except for somewhat increased apparent compressibility of the nanodiamond sample (Fig. 39a). Only slight increase in broadening of the Bragg reflection with an increase in pressure indicates a generation of only limited *micro*-strains in the diamond powders, with somewhat higher strains level in that with nano-sized particles (Fig. 39a). The effect of pressure on SiC grains is much stronger (Fig. 39b). In the presence of a coarse, micro-sized diamond powder the compression of SiC nanograins is much lower, in the presence of nanodiamond – much higher than that of bulk SiC. Consistent with the above, in the mixture with micro-diamond SiC grains develop limited *micro*-strains only, while in the presence of nano-diamond the amount of strain is considerably higher (Fig. 39b). Low apparent compressibility and low concentration of micro-strains in SiC is obviously due to formation of a matrix made from large, micro-sized diamond grains and accommodation of the small SiC crystallites in the pores of the compact. In the mixture with small size diamond, its nanoparticles (which are much harder than SiC) act merely as a medium transferring stresses between individual SiC grains. In the presence of the same-size diamond powder, SiC develops a lot of *micro*-strains, and its compressibility apparently increases relative to the bulk material (Fig. 39b). Similarly, higher content of microstrains and increased compressibility implies, that nano-sized diamond is softer than large size crystals of the material. These phenomena will be discussed in more details in Secs. 16 and 17.

13. Determination of *macro*- and *micro*-strains from asymmetric Bragg reflections

It is often observed that the shape of the Bragg reflections becomes asymmetric under pressure. That effect is the result of a presence of *micro*-strains in the material. The asymmetry of the reflections requires some special procedures to determine their position and the corresponding lattice parameters. As long as the lattice parameters

are used to evaluate *macro*-strains present in the material, the specific method of the evaluation is not critical. It should, however, be applied consistently throughout the study, and its shortcomings should be taken into account. We examined changes of the lattice parameters and peak widths with pressure using two procedures:

1. The peak positions were measured at the weighted center of intensity of the reflections. For symmetric reflections the center of intensity coincides with the peak maximum, for asymmetric ones the weighted center is shifted relative to the maximum. FWHM was used as the peak width.
2. The asymmetric peak shapes were approximated by a combination of two simple shape functions: Gaussian and Lorentzian. Consequently, changes of the lattice parameters and widths (FWHMs) of the peaks were traced separately for each of the peak shape components (c.f. application of splitting Bragg reflections into the Gaussian and Lorentzian components for analysis of strains in copper single crystals [91]).

Figure 40 shows an example of (111) Bragg reflections of SiC measured under the pressure of 0, 3, and 9 GPa. Without an external pressure the positions of the peak maxima and the weighted peak centers coincide (Fig. 40). With an increase in pressure, the weighted center of the peak shifts towards the right (towards smaller d-values) relative to the peak maximum. The positions of the Gaussian and Lorentzian components of the peak move to the left and right side of the peak maximum, respectively. The increase in the shift of the peak experimental positions with an increase in pressure is accompanied by an increase in the asymmetry of the Bragg reflection (Fig. 40). Based on our theoretical calculations of diffraction patterns we suggest, that a split of a single Bragg reflection into two components can be interpreted as a result of a presence of several fractions of the same material with differently strained lattice in the sample. As shown in Fig. 38 and discussed in Sec. 14.1, the asymmetry of the peaks can be interpreted as a change of the ratio of the components of the reflections, the Gaussian and Lorentzian shape functions. (Note that in Fig. 37 we combined two Gaussian functions; in general, any combination of Gaussian and Lorentzian profile functions can be applied.) By the right combination of these basic shapes, the (asymmetric) shape of the Bragg reflections can be simulated. An example of the reflection calculated for a more a complex model of nanocrystalline powders, with non-uniform distribution of strains in grains of different size is shown in Fig. 41. When the grains have identical, uniform structure and size (6 nm in diameter), the Bragg reflections have the Gaussian type shape (Fig. 41a). A mixture of 1 to 10 nm grains with the average size of 6 nm and uniform and identical lattice gives Bragg reflections which are a combination of the Gaussian and Lorentzian shape, both component peaks being at the same position (Fig. 41b). When the model mixture has the same grains as in Fig. 41b but the lattice parameters are from 4.30 Å for the smallest to 4.41 Å for the largest grains, the resulting shape of the Bragg reflections is also approximated by a combination of the Gaussian and Lorentzian shape components but at different positions in the diffraction pattern (Fig. 41c).

The experimentally obtained shapes of the Bragg reflections of nanocrystalline SiC powder compressed isostatically showed in Fig. 40 match closely those calculated for the model presented in Fig. 41. From that we conclude, that our experimental

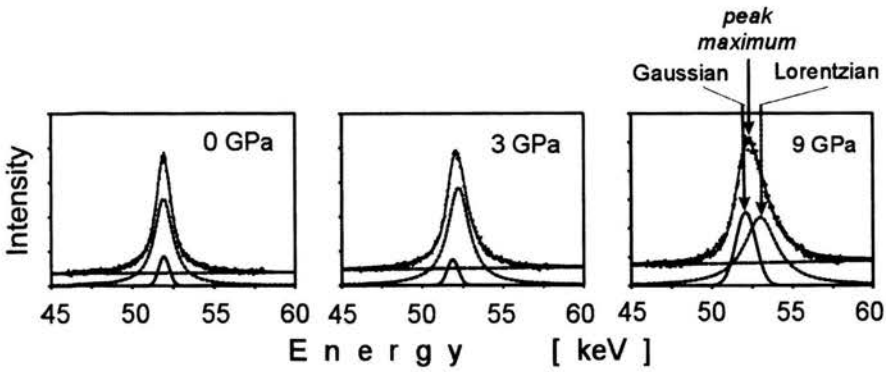

FIGURE 40. (111) reflections of 10 nm SiC crystals obtained under different pressures.

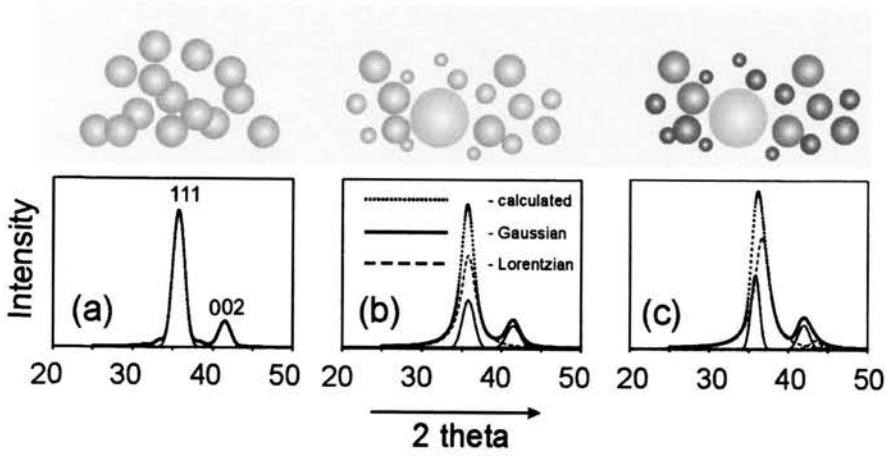

FIGURE 41. Calculated theoretical diffraction patterns of SiC nanocrystals (dotted lines). Solid and dashed lines – Gaussian and Lorentzian curves, respectively. (a) uniform grain size (6 nm) powder; (b) a mixture of 1 to 10 nm grains powder with the average grain size of 6 nm; (c) a mixture of 1 to 10 nm grains with the average size of 6 nm and the lattice parameters from 4.30 Å for the smallest to 4.41 Å for the largest grains.

sample under compression can be described well by a model of powder containing several fractions of grains, each at a different degree of compression: smaller grains being compressed more than the larger ones. This conclusion can be made more general by saying that smaller objects (grains, domains) accumulate more stress than larger ones. Such interpretation is consistent with distribution of strains in materials predicted theoretically based on the theory of elasticity [41]. A schematic model of distribution of strains (stress fields) in a system of closed packed spheres for different (isostatic) pressures is shown in Fig. 42. As discussed already in Sec. 12,

an external load applied to a porous sample propagates in the material through contact points between individual grains. At low pressures/low compression the contact areas between the grains are small and, therefore, extreme stresses and, subsequently, *micro*-strains develop at the contact points (Fig. 42b). The shape of the formed stress fields is approximately spherical (c.f. [41]). With an increase of the applied external stress the contact areas increase. Simultaneously the gradients of the stresses decrease, but the extend of the stress field originating at the grain surface becomes quite extensive (Fig. 42c). In general, the areas with stronger local stresses are always smaller than those where the stress is weaker. This conclusion is consistent with the distribution of stresses in a powder presented in Fig. 41, where the smallest grains show the largest strains. The strongly compressed parts of the grains can be regarded as the domains of the same material with different lattice parameters. The smallest domains have the largest strains and the larger ones accommodate less strain. It is illustrated schematically in Fig. 42c with spheres of different diameter. In a porous material under external stress, areas (domains) under different stresses exist. We suggest that a powder grain under nonuniform stress conditions resembles a cluster of grains with different diameters and different strains (compare Fig. 41).

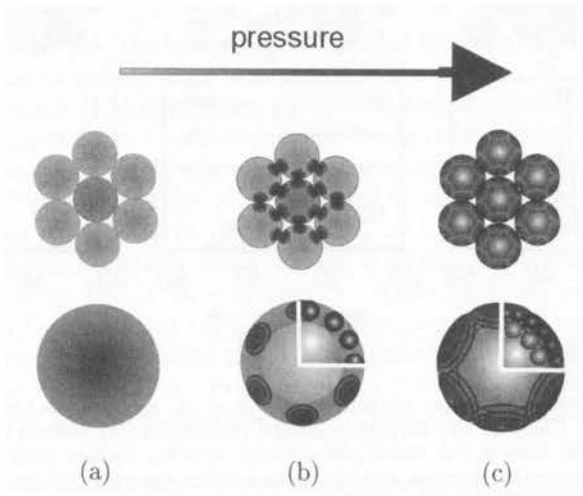

FIGURE 42. Tentative model of distribution of microstrains developed in individual powder particles densified under isostatic pressure conditions: (a) before compression; (b) under low pressure; (c) under high pressure. Upper models – assemblies of grains, lower models – individual grains. The lines within the grains are isostress lines.

To verify the above model of generation of strains we investigated the distribution of stresses in a series of SiC and GaN nanopowders with different grain size compressed under isostatic pressure conditions.

14. Experimental verification of models of distribution of strains in nanocrystalline SiC densified under very high isostatic pressures

The SiC powders for our experiments were provided by D. Keil [92] and GaN by J.F. Janik [93]. As the first approximation, in this section we assume that nanocrystal is a single phase material with (initially) a perfect crystal lattice. We have found that similar nanopowders can show symmetric or asymmetric shape of Bragg lines under pressure. Therefore both types of the experimental data are analysed below.

14.1. Analysis of distribution of strains in nanocrystals with asymmetric Bragg reflections

Development of strains was determined from the diffraction patterns obtained at different pressures up to the maximum of 40 GPa. The change of the lattice parameter with pressure in SiC, based on the position of the maxima of (111) Bragg reflection, is shown in Fig. 43a. In the low-pressure range (up to 3-4 GPa) the lattice parameter decreases very steeply with an increase in pressure (Fig. 43a). The compression of the sample resembles that of such a soft material as gold. In the pressure range from 4 to 15 GPa the apparent compression of SiC is very low (the compression of the material resembles that of diamond). At pressures higher than 15 GPa the compressibility assumes an intermediate value, smaller however than that corresponding to the bulk compressibility of SiC. The dependence of the lattice parameter on pressure is similar for all grain sizes except for the middle pressure range where compression is higher for powders with smaller grains. Due to isostatic, as opposed to hydrostatic nature of the applied pressure, the observed changes of the lattice parameter may be attributed to the elastic properties of the crystal lattice demonstrated by *macro*-strains, but also to a presence of strong *micro*-strains in the sample material that may also affect the positions of the Bragg reflections (c.f. Figs. 38 and 39).

The alternate way of the data elaboration is based on the analysis of the diffraction data separately for the Gaussian and Lorentzian components of the Bragg reflection (c.f. Sec. 13) and presented in Fig. 43b. The two components of the Bragg peak behave very differently under pressure. Up to three pressure ranges can be distinguished. At lower pressures, the compression of the Gaussian component is always much smaller than that of the Lorentzian one (Fig. 43b). Apparently the very strong compression exhibited by the Lorentzian component is associated with the surface of the grains. Extreme stresses develop at inter-grain contact points (c.f. Fig. 37), and at lower pressures the local stress is much higher than the average pressure in the sample volume (c.f. Fig. 42). The strong compression of the SiC lattice at the grain surface occurs simultaneously with an increase of the contact area of the grains. As the external stress increases, the contact area between the grains increases and further increase of the external stress leads to a much smaller increase of *micro*-strains (c.f. Fig. 36). (The appearance of specific pressures where a discontinuous change of the compression properties is observed might be associated with a local plastic deformation, better packing of grains due to gliding, etc. Discussion of such phenomena is outside the scope of these lectures). A strong compression

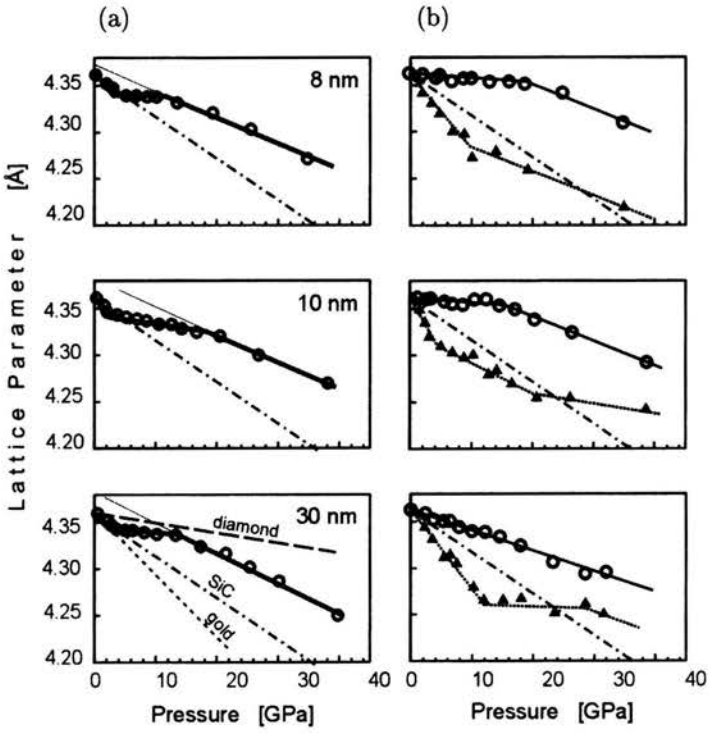

FIGURE 43. Lattice parametr of SiC nanocrystals as a function of isostatic pressure for different grain sizes: (a) solid lines and open circles – lattice parameters as-determined from the position of the maxima of (111) Bragg reflections; (b) lattice parameters as-determined from the positions of the Gaussian (dashed lines and open tringels) and Lorentzian (dotted lines and solid triangles) components of the peak shape functions. Dash-dotted lines – regular compression curves (SiC).

at the surface (where the elastic energy of the lattice is accumulated) makes the inter-grain boundaries much harder than the interior of the grains. As a result the surface layer, which in a dense material merges with the adjacent surface layer into an inter-grain boundary, becomes even harder and protects the interior of the grains from the external stress. This situation is similar to that shown in Fig. 39 for compression of a mixture of powders of different hardness. The Gaussian component of the Bragg reflections, which provides information on the crystal lattice in the grain cores, shows only limited compression at low pressures due to a presence of the barrier of very strongly compressed (and, thus, extremely hard) grain boundary (Fig. 43b). These boundaries form a kind of a very hard matrix (skeleton) like the one shown in Fig. 42.

The effect of the surface layer hardening on compression of the grain interior is not observed for the large grain (30 nm in diameter) sample (Fig. 43b). This is apparently due to the fact that the ratio of the surface atoms to the total number of atoms in the sample with 30 nm grains is about 10 times less than that in the 8 and 10 nm size grains. As a result, the protective effect of the hardened surface

layer is much less effective for larger grains. This is consistent with the fact that the largest difference between the Gaussian and Lorentzian plots is observed for the smallest grains. This difference decreases with an increase in the grain size and at high pressures (Fig. 43b).

As shown above, experimental determination of a change of the lattice parameters with a change in (isostatic) pressure can provide information on distribution of strains in nanopowders. That information is primarily qualitative. A quantitative evaluation of the results requires a careful scrutiny: the compression of the lattice parameters for all our SiC samples is, except in the initial stage of compression, much smaller than that corresponding to the bulk modulus of the material; this applies to both the Gaussian and Lorentzian components. (The above observations may not apply to all nanocrystals.) This is a strong indication that in this particular experiment (c.f. Fig. 43a) a part of the external energy has been accumulated in the sample in a form not detectable by the diffraction experiment. Thus, the information on the material's behavior available from our experiment is incomplete and may lead to erroneous conclusions. At the present stage of our study, we did not even attempt to evaluate the real compressibility of the examined nanocrystals.

A presence and magnitude of microstrains can be evaluated from broadening of the Bragg reflections. However, the width of a peak is not well defined for asymmetric shapes, and does not carry any unambiguous information about the material structure (the broadening may be due to a presence of *micro*-strains, but may also come from a presence of large fractions of the same material compressed to a different degree, c.f. Figs. 38 and 39). Therefore, no quantitative information on strains can be derived from such quantity. For the above reason no quantitative interpretation of *micro*- and *macro*-strains from the present experimental data has been attempted.

The nanocrystals used for the above experiments were as-synthesized SiC powders obtained using the flame technique [91]. Similar experiments using nanocrystalline SiC fabricated with a different technique might give different results.

14.2. Analysis of distribution of strains in nanocrystals with symmetric Bragg reflections

For these studies two materials, very hard SiC, and much softer GaN were selected. The SiC powders were pre-annealed prior to the diffraction experiments. The samples had the average size of the particles from 2 to 30 nm. The SiC samples were cubic with one-dimensional disorder (stacking faults). GaN samples with the smallest grains show the structure similar to that of SiC, the larger grains were hexagonal (wurtzite). It was found that the Bragg reflections measured under isostatic pressure conditions have symmetrical or nearly symmetrical shapes. Symmetry of Bragg reflections is an indication that distribution of strains in the material is homogenous and both *macro*- and *micro*-strains in the samples, using positions and width of the reflections, respectively, can be determined. The d spacings were calculated from the positions (measured at the weighted center of intensity) of the (111) Bragg reflections. For large-grain GaN samples with hexagonal structure (002) reflections were analyzed. The relative change of the lattice parameters (the measure of *macro*-strains) and FWHM (the measure of *micro*-strains) with pressure for SiC powders

with different grain size is shown in Figs. 44a and 44b, respectively. The apparent effect of pressure on *macro-* and *micro*-strains generated in SiC depends on the average size of the grains. A very strong decrease of the as-measured lattice parameters with increasing pressure (up to 3-4 GPa) irrespective of the grain size occurs. It is followed by a pressure range (up to 6-12 GPa) of nearly constant value of the lattice parameter for all grain sizes. The compression curves for larger grains are similar to the one shown for 30 nm crystals. Above the pressures marked by the arrows, the compression of the SiC nanopowders is the same as that corresponding to the bulk modulus of SiC, except for the smallest grains (2 and 4 nm, Fig. 44a). In the initial, non-linear parts of the compression curves (Fig. 44a) the changes of the lattice parameter do not correspond to the lattice compression of SiC but to generation of *micro*-strains reflected in broadening of the Bragg reflections (Fig. 44b). At corresponding pressures the width of the Bragg peaks shows an initial strong increase until it "stabilizes" with none or a very limited further increase with an increase in pressure. From this point on the compression of the samples represented by the change of the lattice parameters agrees well with the compressibility of SiC. The compression of the smallest grain powders (2 and 4 nm in diameter) does not reach that of the other samples until the pressure of about 40 GPa. Also, the *micro*-strains in the smallest grains are building up even at pressures around 40 GPa (Fig. 44b).

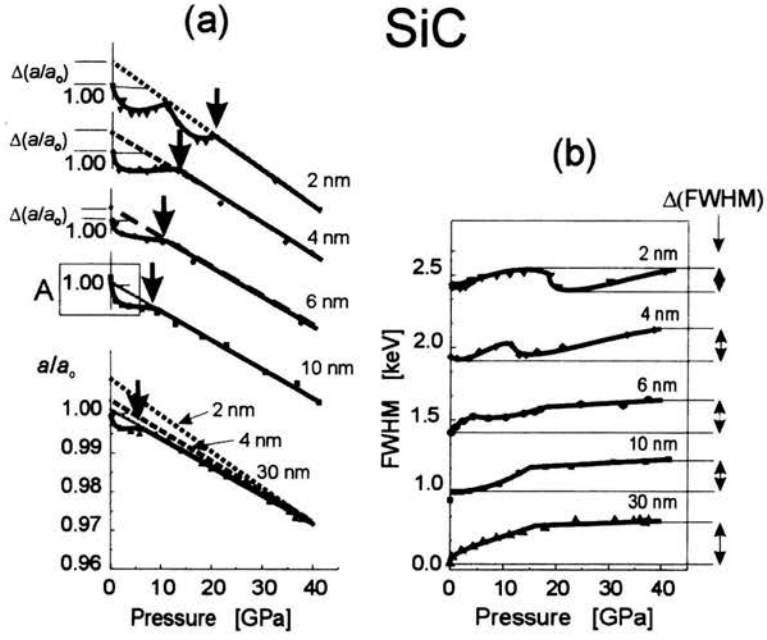

FIGURE 44. Effect of pressure on the structure of SiC nanocrystals for different size grains: (a) relative change of the interplaner spacings (the arrows mark the upper limit of major deviations from the regular compression curves); (b) change of FWHM of the Bragg reflections.

A clear similarity between the results shown in Figs. 43 and 44 exists: in both cases a presence of several compression ranges are observed. However, obvious differences between the results exist too: the slopes of the curves change at different pressures; in Fig. 44a a compression of the lattice above 25 GPa is observed; the apparent compressibility observed in Fig. 43 is much less than that observed in Fig. 44a. The differences are apparently due to a different pre-treatment of the source materials (annealing of the powders of the latter experiments at 400°C under vacuum prior to the measurements). That implies that the difference in the compression curves between these experimental series is due to the grain surface phenomena. In nanograins a few nanometers in diameter the number of atoms associated with the surface is comparable to those located in the interior of the grains. Since the atoms adsorbed at the surface affect the distribution of strains in the surface layer, removal of the adspecies by vacuum annealing may be expected to affect the grains and their dependence on the external pressure.

The effect of pressure on the lattice parameters and broadening of the Bragg reflections for GaN samples is shown in Fig. 45. At the first sight, the effect of pressure on GaN nanocrystals appears similar to that observed for SiC samples (Fig. 44): a steep decrease in the lattice parameter with the initial increase in pressure is followed by leveling off or even some increase as the pressure increases. However, major

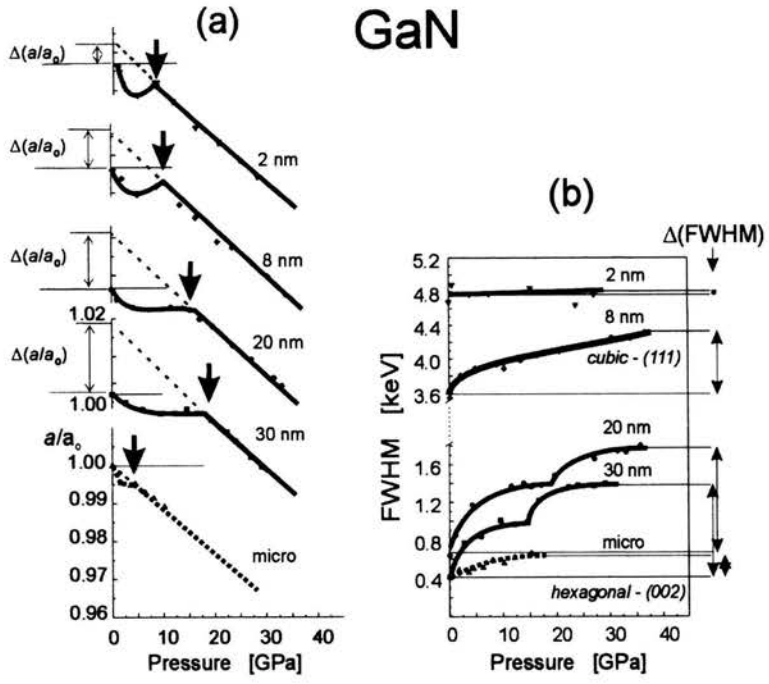

FIGURE 45. Effect of pressure on the structure of GaN nanocrystals for different size grains: (a) relative change of the interplaner spacings (the arrows mark the upper limit of major deviations from the regular compression curves); (b) change of FWHM of the Bragg reflections.

differences between the materials' properties exist. For large SiC grains non-linearity of compression ends at the presure of several GPa and is followed by a regular, elastic compression of the lattice (Fig. 44a). For GaN similar non-linear range is observed for the largest and smallest grains. The largest range of the non-linear change of the lattice parameter with pressure (i.e. in the region of small compression) is for the smallest nanograins of SiC but for much larger, 30 nm grains of GaN. The offset of the straight compression line from the bulk compressibility of the material, $\Delta(a/a_0)$, is the largest for the smallest SiC grains and decreases with an increase of the grain size, while such deviation in GaN increases from 2 to 30 nm grain powders (Figs. 44a and 45a, respectively).

The character of change of broadening of the Bragg reflections (i.e. the development of *micro*-strains and their distribution) with pressure in SiC clearly depends on the grain size. The total increase of width of the reflections over the pressure range from 0 to 40 GPa decreases with the grain size (Fig. 44b). (The complex shape of the curves in Fig. 44b can be explained by agglomeration of powders in the sample; this topic is not discussed further in this work). This means that, of the total energy accumulated in the material under external stress, the portion of the total energy accumulated in the form of *micro*-strains decreases with a decrease in the grain size. That phenomenon can be explained by the fact that in a powder with smaller grains the total number of contacts between individual grains is larger and, therefore, the gradients of the local stresses (and, thus, *micro*-strains) are smaller. Accordingly, the increase of the width of the Bragg reflections with an increase in pressure is smaller. Different than in SiC, no *micro*-strains are present in the smallest GaN grains in the entire pressure range of compression (Fig. 45b). However, opposite to SiC, a very strong increase in the width of the Bragg reflections with an increase in pressure is observed for larger grains (8, 10, and 30 nm). Unlike for SiC, a strong increase of width of the Bragg lines in GaN is not due to an increase of *micro*-strains. This increase is due to two processes: (i), in the pressure range up to 15-20 GPa a generation of stacking faults occurs, and is followed by, (ii), a decrease of the grain size by breaking individual crystals into plates and needles as discussed in a separate paper [53].

Compressibility of a material is the relative change of the lattice parameter per unit pressure change (c.f. Sec. 7) and is constant in the elastic region. The compressibility of our materials can be determined from the linear portion (for pressures higher than those marked by the arrows) of the curves shown in Figs. 44a and 45a. In that pressure range the entire increase of the stress applied from the outside is accumulated as the elastic energy of the lattice in the form of *macro*-strains and leads to shifts of the Bragg reflections towards smaller d-values. At lower pressures, a generation of complex *micro*-strain fields and activation of other processes like formation of stacking faults occurs. That leads to a part of the stress being relaxed by these processes and only a portion of the applied stress is effectively transferred to the interior of the grains and shows in the diffraction pattern. As a result, the positions of the Bragg lines do not correspond to the specific values of the lattice parameters, and no compressibility of the sample can be determined in that range (c.f. Figs. 38 and 39, Sec. 12). When less of the external stress is used for generation of *micro*-strains, higher fraction of the external stress is transferred to the interior of the grains and to the compression of its crystal lattice.

As the density of the sample increases, the total area of contacts between the grains increases and the amount of *micro*-strains levels off. At sufficiently high pressures the material approaches closely the theoretical density and the lattice parameters determined from the Bragg lines correspond to those calculated directly from the compressibility of the material.

15. Hydrostatic versus isostatic compression

As discussed in previous sections, determination of compressibility of a material requires that no *micro*-strains form in the sample during the measurements. This can be accomplished under hydrostatic pressure conditions, i.e. by using a liquid pressure medium. Under such conditions the shape and width of the Bragg reflections of a single-phase crystalline material do not change with pressure. Only under such conditions the real lattice parameters under pressure can be measured and the real lattice compressibility can be determined. A dependence of compressibility of nanomaterials on the grain size as well as the effect of the grain size on high-pressure phase transformations were reported [84]-[88]. As showed in previous sections, interpretation of high-pressure diffraction experiments on nanocrystals of SiC and GaN is not unambiguous and requires a careful scrutiny. An experiment performed under hydrostatic pressure conditions may be expected to provide unique compressibility data for such materials. In Figs. 46 and 47 the results of high-pressure diffraction ex-

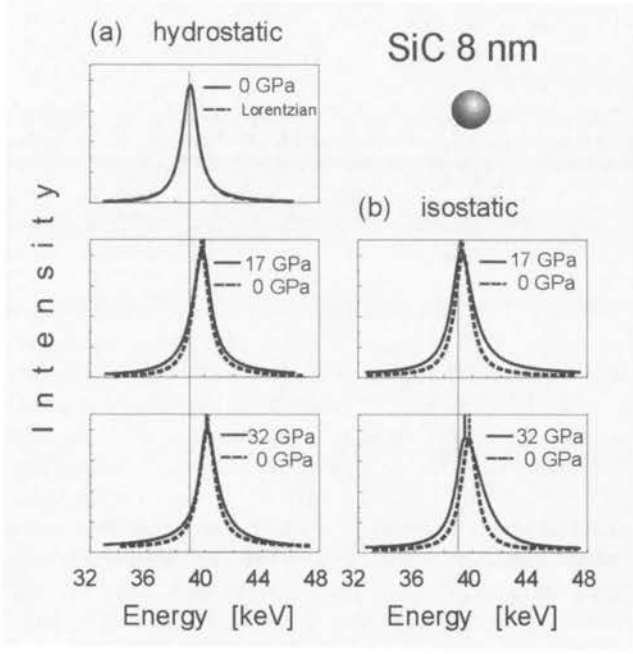

FIGURE 46. Change of the shape of (111) Bragg reflections with pressure for 8 nm SiC crystals: (a) hydrostatic pressure, (b) isostatic pressure.

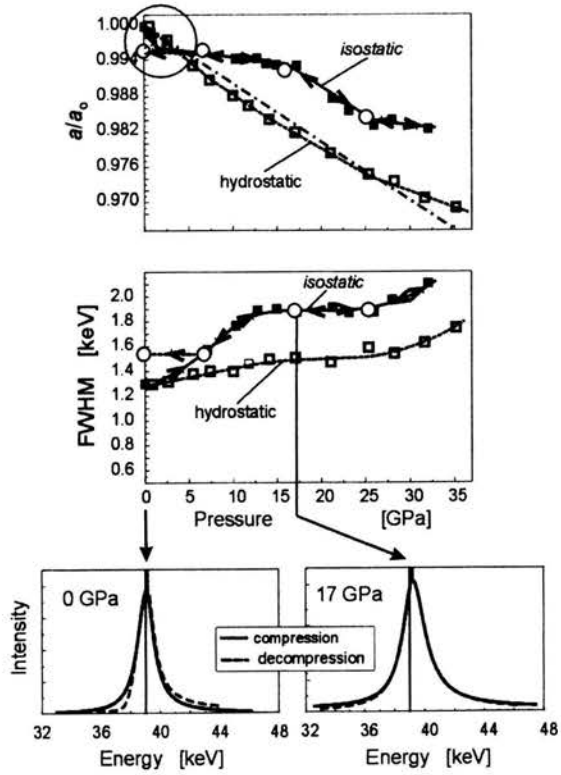

FIGURE 47. Effect of pressure on strains in 8 nm SiC crystals. Solid squares and solid lines – isostatic, open squares and dotted lines – hydrostatic, circles – points obtained during the samples decompression. (a) and (b), relative changes of the lattice parameters and the reflection widths (FWHMs), respectively; (c) Bragg reflections during compression and decompression stages of the process. Dash-dotted line – regular compression curve of SiC.

periments on 8 nm SiC powders obtained under isostatic and hydrostatic conditions are shown. The shape of the Bragg reflection of the starting material ($P = 0$) fits closely the Lorentzian function (Fig. 46a). For a reference, this reflection is shown in the other graphs of Fig. 46 with its maximum placed at the position corresponding to the weighted center of intensity of a given reflection. As seen in Fig. 46, the Bragg reflections broaden both under hydrostatic and isostatic pressure, although the broadening is more pronounced under the latter. Under both conditions the reflections measured under pressure are slightly asymmetric. The positions of the reflections maxima are different than those of their weighted intensity centers. Compression curves based on the weighted peak positions and the FWHM values for both iso- and hydro-static conditions are shown in Fig. 47. As seen, neither for iso- nor for hydro-static pressure conditions the compression of the lattice measured from the weighted intensity positions of the Bragg reflections match the lattice compressibility of SiC in the entire pressure range. Both plots are approximately parallel to the

bulk compression curve of SiC in the middle pressure range, but deviate from it at low and high pressures. Above 25 GPa no compression of the lattice parameters (a hardening of the samples, more pronounced under isostatic conditions) is observed (Fig. 47a).

To verify the equilibrium nature of the lattice compression, we have measured the diffraction patterns at several pressures during the sample decompression. Both (for increasing and decreasing pressure) sets of the experimental points are consistent and do not show any hysteresis over most of the pressure range (Fig. 47). A presence of small amount of residual stress in the decompressed powder is demonstrated by a strong asymmetry of the Bragg reflection in the material after decompression; no difference in the shape of the Bragg reflection measured at a higher pressure (17 GPa) during compression and decompression is observed (Fig. 47c). That is a clear indication that during compression of the powders only elastic energy accumulates in the material: the material "recovers" after the stress is removed. The development of *micro*-strains can be derived from the broadening curves. The shape of the curves for isostatic and hydrostatic pressures is similar but the change of the peak width is much larger for the former conditions (Fig. 47b). The initial increase in FWHM values levels off at about 12 GPa. Further increase in pressure, up to about 25 GPa, apparently does not generate any additional microstrains and the width of the reflections remains unchanged (Fig. 48b). Above the pressure of 25 GPa the broadening of the Bragg reflections increases again (Fig. 47b) what coincides with a decrease in the rate of compression of the lattice (Fig. 47a). The two experiments presented above show that neither under isostatic nor under hydrostatic conditions do SiC nanocrystals show unique, unambiguous compressibility data.

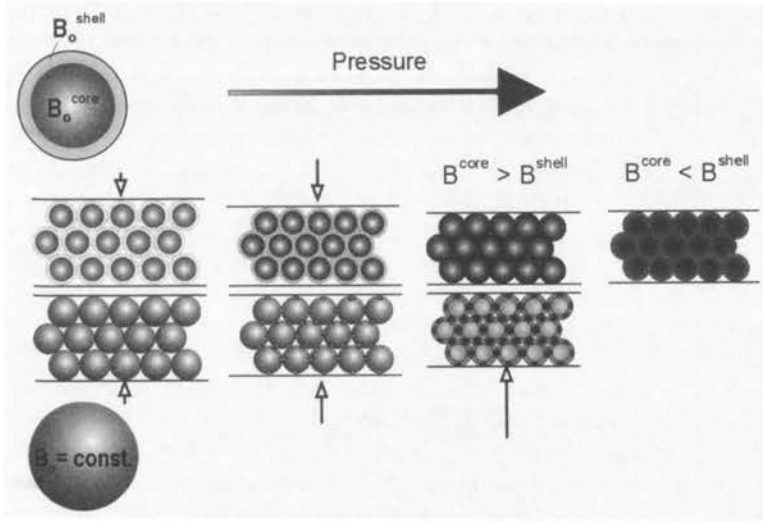

FIGURE 48. Distribution of strains under isostatic pressure. (a) two-phase (core-shell) powder grains; (b) grains with a uniform initial structure.

16. Application of core-shell model for interpretation of h-p diffraction experiments on SiC nanocrystals

So far we attempted to interpret the change of the diffraction patterns of nanocrystals measured under high pressures as a result of generation of strains in a well-defined, uniform crystallographic phase material. An alternate interpretation of the diffraction data of nanocrystals is based on a two-phase model of nanocrystalline grain. Such model assumes that the atomic structure and properties of the grain core and of the surface are different. Consequently, the elastic properties of the grain cores and surfaces are different too and the behavior of such nanocrystals under pressure can be interpreted as being the result of a presence of two phases with different elastic properties. Below we present some preliminary results on application of such a model in our studies.

In a simple core-shell model of nanocrystals it is assumed that the core has a well-defined structure (e.g. a pure cubic structure in SiC). The grain core is surrounded by a surface shell with its structure similar to that in the core but compressed or expanded relative to the relaxed lattice. It is obvious that the elastic properties (bulk modulus B_0) of the surface shell (B_0^{shell}) are different than the compressibility of the crystal lattice of the grain core (B_0^{core}).

The mechanism of compression of a powder of spherical grains with a two- and one-phase structure is illustrated in Figs. 48a and 48b, respectively. The surface shell (model (a)) can be either harder or softer than the grain core. Under external stress the compression of the surface shell will be respectively smaller or larger than that of the core. As discussed in Sec. 7, the compression proceeds linearly with an increase in pressure in the elastic region and hardens (its bulk modulus increases) at sufficiently high pressures, Sec. 14. When the surface shell is softer than the core, the surface compresses under external stress more than the core. The strong compression of the surface shell leads to hardening of the grain surfaces. Those surfaces form a network of grain boundaries constituting a kind of a matrix embedded with the grain cores. This matrix of grain boundaries hardens under stress and accommodates most of the applied external stresses and, thus, the stress transferred to the grain cores becomes significantly reduced. As a result, the cores are "undercompressed" – less compressed than expected from the average pressure in the sample volume (Fig. 48a, the model with $B_0^{\text{core}} > B_0^{\text{shell}}$). The matrix of the grain boundaries may be expected to have some strength limitations above which it would break up and allow for a more direct transfer of the external stress to the grain cores. At sufficiently high pressures the bulk moduli of the core and surface components may be expected to become equal and the sample to assume the character of a uniform phase material. (The pressure at which the bulk moduli of different fractions become equal depends on the surface of the grains. This could explain why the same material prepared differently shows different compression properties, c.f. Figs. 43 and 44a).

The above postulated mechanism of hardening of the surface shells of the grains, and the resulting formation of hard boundaries between the grains is consistent with the model of a very strong local strain fields generated at the contact points between the grains which we applied for the analysis of the diffraction experiments showing a strong asymmetry of the Bragg reflections (c.f. Sec. 14.1). We split the Bragg reflections into their Gaussian and Lorentzian components receiving two compression

plots (c.f. Fig. 43b). A comparison of the distribution of strains in strongly compressed powders of one phase and core-shell (with $B_0^{\text{core}} > B_0^{\text{shell}}$) grains, Figs. 48b and 48a, respectively, indicates that in each case a similar distribution of strains in grains compressed under isostatic pressure conditions may be expected. That implies that investigation of compression under isostatic pressure conditions does not allow to distinguish between one and two-phase nanocrystalline grains. The actual type of the structure can be identified by performing related experiments under both isostatic and hydrostatic pressure conditions (c.f. Fig. 47).

Compression curves of one-phase grains under hydrostatic pressure conditions should yield a change of the lattice parameters corresponding to the lattice compressibility of the material. In the experiment showed in Fig. 47 the compression of nanocrystalline SiC under hydrostatic pressure does not follow that expected from the compressibility of the material. Also, a change of the *micro*-strains with a change in pressure similar to those found under isostatic pressure is observed. A two-phase grain of SiC nanocrystal with different elastic properties of the grain core and the shell should yield, under hydrostatic pressure, a diffraction pattern similar to that presented in Fig. 38. Assuming that the grain core and the shell constitute two phases with different elastic properties, the diffraction pattern of such material will be a superposition of the diffraction patters of the constituent phases. The compression curves will provide the average compression data. The broadening of the Bragg reflection will not, however, be due to a presence of *micro*-strains, but to the overlap of the reflections from the two fractions.

The above analysis and our conclusion that nanocrystals are two- not one-phase materials require further verification. Additional support of this model comes with the application of our concept of the "apparent lattice parameter", *alp* [47, 48]. This quantity replaces the "lattice parameter" in the description of the atomic structure of nanocrystals examined with powder diffraction techniques. The concept of *alp* was already presented in several papers so here we limit ourselves to only a brief introduction of the method.

17. Application of the *alp* concept for interpretation of h-p diffraction experiment

During our early investigations we found that the lattice parameters calculated from powder diffraction data obtained for very small crystallites show a dependence on the diffraction vector Q. As a consequence, we introduced the *alp* quantity which is the lattice parameter calculated for individual Bragg reflections (at its diffraction vector Q each). The characteristic shape of the plots showing a change of *alp* with Q can be used for evaluation of the atomic structure of the surface shell of nanocrystals. As an example, theoretically calculated *alp*-Q plots for four models of SiC nanograin with a core-shell structure are presented in Fig. 49. The models have the same diameter of the grain and the same thickness of the surface shell but different compressive surface strain. A presence of the surface shell leads to a strong decrease of the *alp* parameters calculated for individual Bragg reflections at small Q-values relative to the relaxed lattice (Fig. 49a). From Fig. 49 it is obvious, that the structure of a material showing a dependence of the calculated lattice parameter on the

diffraction vector Q cannot be described using the concept of a unit cell (defined by unambiguous lattice parameters) [46, 47]. For powder diffraction performed *in situ* under high pressure using X-ray radiation the experimentally accessible Q-range is limited to small Q-values ($< 5\,\text{Å}^{-1}$). (In experiments performed in DAC at HASYLAB in the energy dispersive geometry, good statistics for the diffraction data could be achieved only for reflections within the Q-range of 3-4 Å^{-1}). This experimental Q-range of up to 5 Å^{-1} is sufficient for an investigation of the effect of compression of the surface layer with the *alp*-Q plots. Figure 49b shows the part of the *alp*-Q plot available experimentally for our compression experiments. This Q-range is insufficient for evaluation of the compression of the grain cores. To determine the lattice parameter in the core (c.f. our 2-phase model of a nanocrystalline grain, Part I), data from a large ($> 10\,\text{Å}^{-1}$) diffraction range are necessary; for large Q-values the influence of the grain surface layer structure is small and the *alp* values approach that corresponding to the structure of the grain interior (Fig. 49).

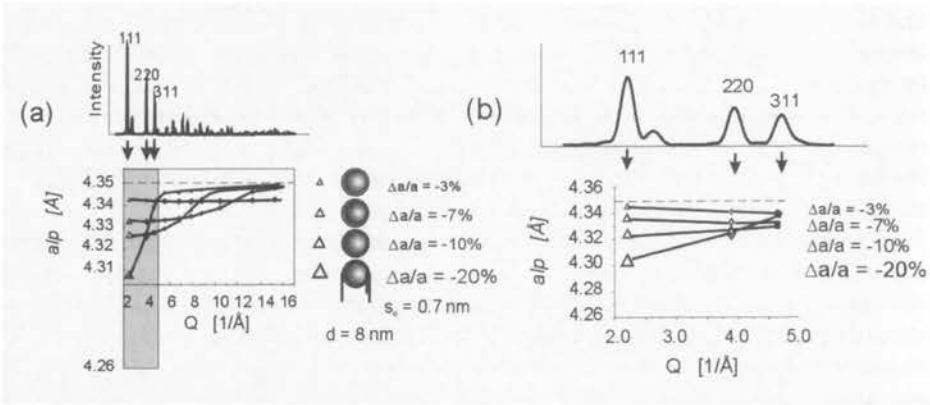

FIGURE 49. Diffraction patterns and *alp*-Q plots for a model of 8 nm diameter SiC nanocrystal with a core-shell structure for different magnitude of (compressive) strain in the surface layer: (a) small Q-range, (b) large Q-range. Dashed lines – the lattice parameter of the core of the model.

The powder diffraction data were obtained for 10 nm SiC grains under both isostatic and hydrostatic compression conditions. The pressure dependence was calculated for three Bragg reflections for each sample. The dependence of the *alp* parameters on pressure is shown in Fig. 50. The change of *alp* is non-linear with pressure, depends on the Q-value (i.e. on the Bragg reflection), and is different for isostatic and hydrostatic conditions. Figure 51 shows the same experimental results versus the diffraction vector Q for different pressures. Based on our numerical simulations of the *alp*-Q plots for nanograins with a core-shell structure we were able to identify and evaluate the strain present in the surface shell of the grains. The strains were determined by matching the experimental results (obtained for large Q-range) and theoretical calculations of powder diffraction patterns for different theoretical models [47, 48]. The results of the calculations for the starting SiC grain with a tensile strain in the shell and the same grain with a compressive strain in the shell are shown schematically in Figs. 51c and 51d, respectively.

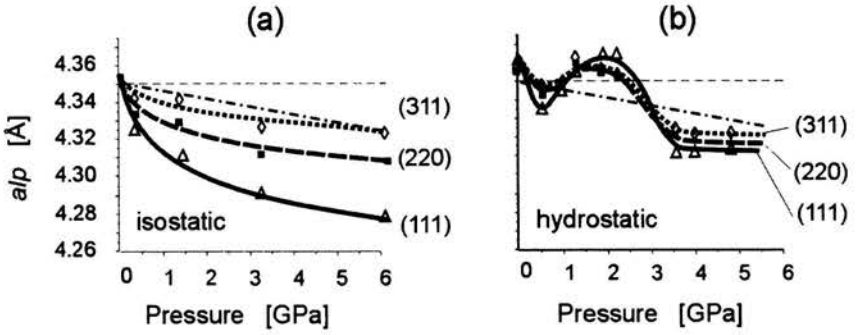

FIGURE 50. Dependance of the apparent lattice parameter 10 nm SiC on pressure for different Bragg reflections. (a) isostatic pressure, (b) hydrostatic pressure. Dashed line – lattice parameter of the microsize material; dashed-dotted lines – lattice parameters calculated from the bulk compressibility of SiC.

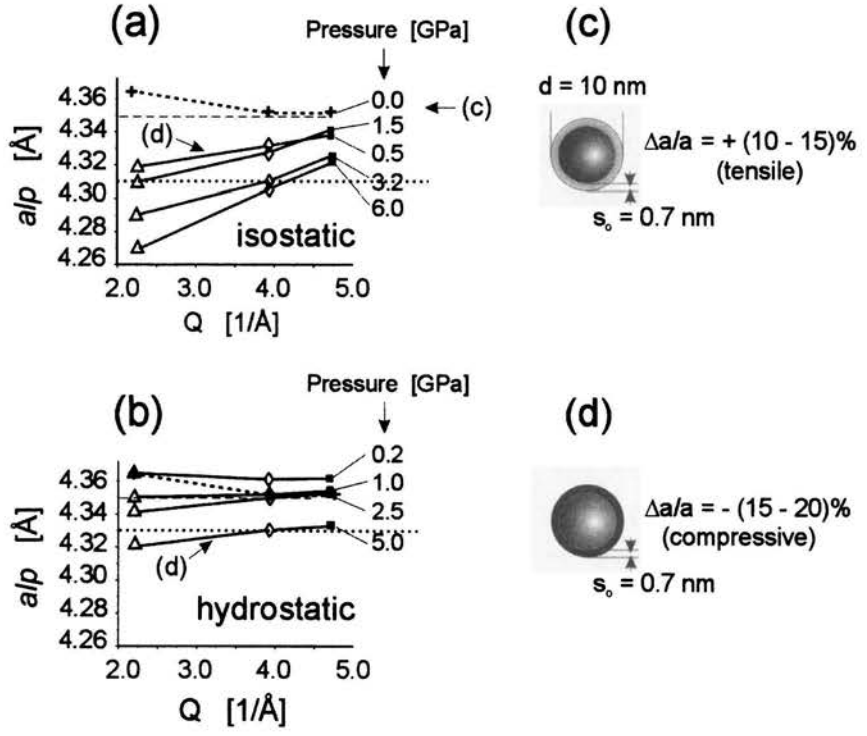

FIGURE 51. *Alp-Q* plots of 10 nm grains nanocrystalline (10 nm grain size) SiC powder measured under pressure. (a) isostatic pressure, (b) hydrostatic pressure; (c) a model of a 10 nm SiC grain of the starting material; (d) a model of the SiC grain with the compression strain in the surface layer. Dashed line – lattice parameter of the core of the model; dotted line – the lattice parameter under the pressure of 5 GPa calculated from the bulk compressibility of SiC.

The analysis of the *alp-Q* plots presented above gives a (tentative) explanation of the h-p diffraction experiments discussed in previous sections. We used a routine procedure of the diffraction data analysis and examined strains generated in nanopowders based on the positions and widths of only one Bragg reflection, (111). In principle, such procedure would be sufficient if the structure of the material was represented by a unit cell. However, as showed in our previous papers [47, 48], according to the *alp-Q* concept the reflections observed at small Q-values are very sensitive to the structure of the surface of the grain (Fig. 49) and, thus, the analysis of a singular Bragg reflection is insufficient for evaluation of strains in nanocrystalline powders. As seen in Fig. 50, the shift of the (111) reflection with pressure is much larger than that for reflections at larger Q-values. In the low isostatic pressure range the extreme stresses generated at the contacts between the grains are confined mostly to the surface of the grains. With an increase in the applied stress a very steep compression of the surface shell leads to a change of the relations between the interatomic distances in the core and the shell. The tensile strain in the surface shell observed in the starting material converts to a compressive strain under the external stress (Fig. 51a) (tensile or compressive type of strain is determined by comparison to the actual lattice parameter in the grain core). This kind of behavior is expected for powders compressed under isostatic conditions, as discussed in Secs. 12 to 14. Our model of generation of extreme strains at the contact between individual grains could explain the presence of *micro-* and *macro-* strains in (initially) isotropic nanocrystals under isostatic conditions. *Micro*strains should be absent in the presence of a pressure medium, i.e. when the grains are not in a direct contact. Surprisingly, identical SiC material compressed under hydrostatic conditions, Fig. 51b, shows behavior similar to that densified under isostatic conditions (Fig. 51a). From that we conclude, that the observed changes of the *alp-Q* plot under hydrostatic pressure result from a difference in the elastic properties of the grain surface and its core; the surface shell with the initial tensile strain has apparently a larger compressibility (smaller bulk modulus) than the grain core, c.f. Fig. 48.

The plots shown in Fig. 51 are based on the *alp* values obtained for relatively small Q-range and cannot be used to evaluate the actual lattice parameters of the cores of the grains (c.f. Fig. 49). The calculated (from the bulk modulus) value of the lattice parameter of SiC compressed hydrostatically under the pressure of 5 GPa is marked in Fig. 51. This value corresponds to the *alp* calculated for the (311) reflection ($Q = 4.7\,\text{Å}^{-1}$) measured under the hydrostatic pressure of 5 GPa. The *alp* values obtained for the same reflection but under isostatic compression are much larger but the first two reflections show much smaller *alp* values (Fig. 51a). For pressures below 5 GPa the experimentally measured *alp* values are similar to those expected from the bulk modulus. However, the first two reflections show smaller *alp*s what suggests that the surface of the grains is suppressed. That indicates that the surface strain in the isostatically-compressed powder penetrates the volume of the grains to a greater depth than when hydrostatic pressure is applied. As a result, in addition to the effect of different elastic properties of the grain core and shell, much larger *micro*-strains are generated in individual grains under isostatic stress conditions. We have to stress out that, due to the limited Q-range of the available

experimental patterns, we could not evaluate the lattice parameters in the interior of the grains.

18. Summary

We performed the analysis of diffraction data obtained for nanocrystalline SiC and GaN powders applying different methods of the data elaboration. We searched for differences in the structure between powders of same material but with different grain size. We examined *micro-* and *macro*-strains and tried to determine the bulk modulus that might be a size-dependent material property. Such dependence might have been due to a presence of internal pressure in as-synthesized nanograins as suggested earlier in the literature (e.g. [82]-[86]). We showed that the densification of nanocrystals always proceeds through several stages and that it is practically impossible to find a unique quantity describing compression of lattice parameters determined from the measured positions of the Bragg reflections. Such behavior was observed during densification of powders without a pressure medium, as well as during compression under pseudo-hydrostatic conditions (with silicon oil as the pressure medium). Under both conditions strong *micro*-strains were generated under pressure. The *micro*-strains strongly affect the actual *macro*-strains that reflect compressibility of the crystal lattice of a given material in the actual pressure range. We suggest that the origin of *micro*-strains is two-fold: (i), a presence of very strong stresses at the contact points between individual grains and, (ii), different elastic properties of the grain cores and shells.

Based on the results of the experimental work presented in these lectures, we cannot unambiguously verify if, in the range from a few nanometers to micrometers, the compressibility of SiC and GaN depends on the size of the grains. We believe, that characterization techniques and procedures developed for particles orders of magnitude larger are inadequate for investigation of nanomaterials. The structure and properties of nanocrystals is too complex to be describable by simple parameters. As we showed earlier [47, 48] a traditional diffraction experiment and its elaboration cannot provide unambiguous information about the real structure of the materials. Therefore, instead of the "lattice parameter" we introduced the so-called "apparent lattice parameter" which can be better suited for very small crystals which have a considerable fraction of their atoms located at the grain boundaries. We also showed that this method of data elaboration, determination of ***alp*** values for different values of the diffraction vector Q, can be applied for a description of changes of the diffraction patterns of nanocrystals subjected to external stresses. Since no single, unique value of the lattice parameter can describe the atomic structure of a nanocrystal, no unique value of compressibility (bulk modulus) that could describe the behavior of nanocrystals under pressure exists either.

We presented only some preliminary results on examination of two nanocrystalline materials, SiC and GaN. Further studies are needed to verify our two-phase grain-core structure model of nanoparticles. Although we showed that the core-shell model explains quite well the development of microstrains both in isostatically and hydrostatically compressed powders, verification of this model requires diffraction measurements performed in a very large range of the diffraction vector Q. Such experiments require application of neutron diffraction techniques.

Acknowledgements

This work was supported by the Polish Committee for Scientific Research – grant PBZ/KBN-013/T08/30, the Polish-German Project POL-00/009 and in part by the EC Grant "Support for Centers of Excellence" No. ICA1-CT-2000-70005, DESY-HASYLAB Project II-99-053, ESRF Project HS-1463.

S. Stel'makh gratefully acknowledges support from the Roman Herzog Program of the Alexander von Humboldt Foundation.

Part I of these Lecture Notes are based on the original, partly published results obtained in collaboration with: E. Grzanka[1,2], S. Gierlotka[1], S. Stel'makh[1], R. Pielaszek[1,2], U. Bismayer[3], J. Neuefeind[4], H.-P. Weber[5] and W. Palosz[6].

Part II of these Lecture Notes are based on the original, partly published results obtained in collaboration with: S. Stel'makh[1], E. Grzanka[1,2], S. Gierlotka[1], R. Pielaszek[1,2], U. Bismayer[3], P. Zinn[7], S. Werner[8] and W. Palosz[6].

References

References for Part I (mainly) and Part II

1. H. FUJITA, On the small atomic clusters dispersed in solids, *Materials Transactions, JIM*, Vol.38, No.8, pp.659-667, 1997.
2. H. FUJITA, Atom clusters and their related phenomens, *J.Electron Microscopy*, Vol.48 (Suppl.), pp.983-994, 1999.
3. H. FUJITA, Studies on atom clusters by ultra-high voltage electron microscopy, *Materials Transactions, JIM*, Vol.35, No.9, pp.563-575, 1994.
4. A.S. EDELSTEIN and R.C.CAMMARATA [eds.], *Nanomaterials: Synthesis, Properties and Applications*, Institute of Physics Publishing, Bristol and Philadelphia 1996.
5. F.E. FUJITA [ed.], *Physics of New Materials*, Springer Series in Materials Science, 1998.
6. M.J. HOWE [ed.], *Interfaces in Materials*, John Wiley and Sons, Inc., 1997.
7. C. SURYANARAYANA [ed.], *Non-equilibrium Processing of Materials*, Pergamon, 1999.
8. Z.L. WANG, *Characterization of Nanophase Materials*, Wiley-VCH, 2000.
9. R.S. AVERBACK, Sintering and deformation of nano-grained materials, *Zeitschrift für Physik*, Vol.D26, pp.84-88, 1993.
10. PH. BUFFAT and J.-P. BOREL, Size effect on the melting temperature of gold particles, *Physical Review*, Vol.A13, pp.2287-2298, 1976.
11. A. INOUE, and K.HISHIMOTO [ed.], *Amorphous and Nanocrystalline Materials: Preparation, Properties and Applications*, Springer, 2001.

[1] High Pressure Research Center UNIPRESS, ul. Sokołowska 29/37, 01-142 Warsaw, Poland.
[2] Institute of Experimental Physics, Warsaw University, ul. Hoża 69, 00-681 Warsaw, Poland.
[3] Mineral-Petrographisches Institut, Uni Hamburg, Grindelalle 48, D-20146 Hamburg, Germany.
[4] HASYLAB at DESY, Notkestr. 85, D-22603 Hamburg, Germany.
[5] SNBL at ESRF, BP 220, Av des Martyrs, F-38043 Grenoble, France.
[6] USRA/NASA-Marshall Space Flight Center, Huntsville, Alabama 35812, USA.
[7] HASYLAB at DESY, Notkestr. 85, D-22603 Hamburg, Germany.
[8] Institut fuer Kristallographie, Uni Muenchen, Theresienstrasse 41, D-20146 Muenchen, Germany.

12. S.B. QADRI, J. YANG, B.R. RATNA, E.F. SKELTON and J.Z. HU, Pressure induced structural transition in nanometer size particles of PbS, *Applied Physics Letters*, Vol.69, pp.2205-2207, 1996.

13. M.R. SILVESTRI and J. SCHROEDER, The size dependence of the high-pressure phase stability of II-VI semiconductor nanocrystals, *Journal of Physics: Condensed Matter*, Vol.7, pp.8519-8527, 1995.

14. S.H. TOLBERT and A.P.ALIVISATOS, Size dependence of the solid-solid phase transition in CdSe nanocrystals, *Journal of Physics*, Vol.D26, pp.56-58, 1993.

15. D. WOLF and K.L.MERKLE, in: D. Wolf. and S. Yip [eds.], *Materials Interfaces: Atomic Level Structure and Properties*, pp.87-150, Chapman and Hall, London 1992.

16. J. HARADA and K.OHSHIMA, X-ray diffraction study of fine gold particles prepared by gas evaporation technique, *Surface Science*, Vol.106, pp.51-57, 1981.

17. C. SOLLIARD and M. FLUELI, Surface stresses and size effect on the lattice parameter in small particles of gold and platinum, *Surface Science*, Vol.156, pp.487-494, 1985.

18. J. WOLTERSDORF, A.S. NEPIJKO and E. PIPPEL, Dependence of lattice parameters of small particles on the size of the nuclei, *Surface Science*, Vol.106, pp.64-69, 1981.

19. P.A. MONTANO, G.K. SHENOY, E.E. ALP, W. SCHULZE and J. URBAN, Structure of copper microclusters isolated in solid argon, *Physical Review Letters*, Vol.56, pp.2076-2079, 1986.

20. S.H. TOLBERT and A.P. ALIVISATOS, The wurtzite to rock salt structural transformation in CdSe nanocrystals under high pressure, *Journal of Chemical Physics*, Vol.102, pp.4642-4656, 1995.

21. F.W.C. BOSWELL, Precise determination of lattice constants by electron diffraction and variations in the lattice constants of very small crystallites, *Proceedings of the Physical Society (London)*, Vol.A64, pp.465-476, 1951.

22. J.-P. BOREL and A. CHATELAIN, Surface stress and surface tension: equilibrium and pressure in small particles, *Surface Science*, Vol.156, pp.572-579, 1985.

23. R.C. CAMMARATA, Thermodynamic model for surface reconstruction based on surface stress effects, *Surface Science Letters*, Vol.273, pp.L399-L402, 1992.

24. R.C. CAMMARATA, Surface and interface stress effects on interfacial and nanostructured materials, *Materials Science and Engineering*, Vol.A237, pp.180-184, 1997.

25. J.J. GILMAN, Direct measurements of the surface energies of crystals, *Journal of Applied Physics*, Vol.31, pp.2208-2218, 1960.

26. C.W. MAYS, J.S.VERMAAK and D.KUHLMANN-WILSDORF, On surface stress and surface tension, II. Determination of the surface stress of gold, *Surface Science*, Vol.12, pp.134-140, 1968.

27. R. SHUTTLEWORTH, The surface tension of solids, *Proceedings of the Physical Society (London)*, Vol.A63, pp.444-457, 1950.

28. A.M. STONEHAM, Measurement of surface tension by lattice parameter changes: theory for facetted microcrystals, *Journal of Physics C: Solid State Physics*, Vol.10, pp.1175-1179.

29. J.S. VERMAAK, C.W. MAYS, and D. KUHLMANN-WILSDORF, On surface stress and surface tension, I. Theoretical considerations, *Surface Science*, Vol.12, pp.128-133, 1968.

30. D.L. BISH and J.E. POST, Modern powder diffraction, *Reviews in Mineralogy*, Vol.20, Mineralogical Society of America, Washington DC 1989.

31. R.A. YOUNG [ed.], *The Rietveld Method*, International Union of Crystallography, Oxford University Press, 1993.

32. H.P. KLUG and L.E. ALEXANDER, *X-Ray Diffraction Procedures*, John Wiley & Sons, 1954.

33. B. BONDARS, S. GIERLOTKA and B. PALOSZ, Program for simulation of diffraction patterns of small particles, *Materials Science Forum*, Vol.133-136, pp.301-306, 1993.

34. R. PIELASZEK, S. GIERLOTKA, S. STEL'MAKH, E. GRZANKA and B. PAŁOSZ, X-ray characterization of nanostructured materials, *Proceedings of the 4th High Pressure School on Chemistry, Biology, Materials Science and Techniques*, Warsaw, 22-25 June 2001, Defect and Diffusion Forum – 2002 [in press].

35. N. COMBE, P. JENSEN and A. PIMPINELLI, Changing shapes in nanoworld, *Physical Review Letters*, Vol.85, pp.110-113, 2000.

36. M.R. FITZSIMMONS, J.A. EASTMAN, M. MUELLER-STACH and G.WALLNER, Structural charecterization of nanometer-sized crystalline Pd by X-ray diffraction techniques, *Physical Review B*, Vol.44, pp.2452-2460, 1991.

37. J. LOEFFLER and J. WEISSMUELLER, Grain-boundary atomic structure in nanocrystalline palladium from X-ray atomic distribution functions, *Physical Review*, Vol.B52, pp.7076-7093, 1995.

38. X. ZHU, R. BIRRINGER, U. HERR and H. GLEITER, X-ray diffraction studies of the structure of nanometer-sized crystalline materials, *Physical Review B*, Vol.35, pp.9085-9090, 1987.

39. S.J.L. BILLINGE and M.F. THORPE, *Local Structure from Diffraction*, Plenum Press, New York and London 1998.

40. TH. PROFFEN and S.J.L. BILLINGE, PDFFIT, a program for full profile structural refinement of the atomic pair distribution function, *J. Applied Crystallography*, Vol.32, 579, 1999.

References for Part II (only)

41. M. EREMETS, *High Pressure Experimental Methods*, Oxford University Press, 1996.

42. B. BURAS and L. GERWARD, Application of X-ray energy dispersive diffraction for characterization of materials under pressure, *Prog. Crystal Growth and Characterization*, Vol.18, pp.93-138, 1989.

43. R. DEFAY and I. PRIGOGINE, *Surface Tension and Adsorption*, Longmans, Green & Co Ltd. 1966.

44. D. WOLF and K.L. MERKLE, in: D. Wolf and S. Yip [eds.], *Materials Interfaces: Atomic Level Structure and Properties*, Chapman and Hall, pp.87-150, London 1992.

45. M.J. HOWE [ed.], *Interfaces in Materials*, John Wiley and Sons, Inc., 1997.

46. D. WOLF and S. YIP [eds.], *Materials Interfaces: Atomic Level Structure and Properties*, Chapman and Hall, 1992.

47. B. PAŁOSZ, E. GRZANKA, S. GIERLOTKA, S. STEL'MAKH, R. PIELASZEK, W. LOJKOWSKI, U. BISMAYER, J. NEUEFEIND, H.-P. WEBER, and W. PALOSZ, Application of X-ray powder diffraction to nano-materials; determination of the atomic structure of nanocrystals with relaxed and strained surfaces, *Phase Transitions*, 2002 [in press].

48. B. PAŁOSZ, E. GRZANKA, S. GIERLOTKA, S. STEL'MAKH, R. PIELASZEK, U. BISMAYER, J. NEUEFEIND, H.-P. WEBER and W. PALOSZ, Diffraction studies of nanocrystals: theory and experiment, *Acta Physica Polonica*, 2002 [in press].

49. R. PIELASZEK, M. ALOSHINA, B. PAŁOSZ, S. GIERLOTKA and S. STEL'MAKH, Modeling of strain distribution in non-hydrostatically pressed nanocrystalline SiC: in situ diffraction study, *MRS Symp. Proc.*, Vol.501, pp.305-310, 1998.

50. B. PAŁOSZ, S. STEL'MAKH, S. GIERLOTKA, M. ALOSHINA, R. PIELASZEK, P. ZINN, TH. PEUN, U. BISMAYER and D.G. KEIL, Evolution of disordering in SiC under high pressure high temperature conditions: in situ powder diffraction study, *Materials Science Forum*, Vol.278-281, pp.612-617, 1998.

51. B. PAŁOSZ, S. GIERLOTKA, S. STEL'MAKH, R. PIELASZEK, P. ZINN and U. BISMAYER, High-pressure high temperature in-situ diffraction studies of nanocrystalline ceramic materials at HASYLAB, *Journal of Alloys and Compounds*, Vol.286, pp.184-194, 1999.

52. R. PIELASZEK, B. PALOSZ, S. GIERLOTKA, S. STELMAKH and U. BISMAYER, A Model of strain distribution in nanocrystalline SiC and diamond at very high pressures: in situ X-ray diffracrtion study and computer modelling, *MRS Symp Proc.*, Vol.538, pp.561-566, 1999.

53. E. GRZANKA, B. PALOSZ, S. GIERLOTKA, R. PIELASZEK, K. AKIMOW, U. BISMAYER and J.F. JANIK, Generation and relaxation of microstrains in GaN nanocrystals under extreme pressures, *Acta Physica Polonica*, 2002 [in press].

54. A.S. EDELSTEIN and R.C. CAMMARATA [eds.], *Nanomaterials: Synthesis, Properties and Applications*, Institute of Physics Publishing, Bristol and Philadelphia, 1996.

55. C. SURYANARAYANA [ed.], *Non-equilibrium Processing of Materials*, Pergamon, 1999.

56. Z.L. WANG, *Characterization of Nanophase Materials*, Wiley-VCH, 2000.

57. A. INOUE, A. and K. HISHIMOTO [eds.], *Amorphous and Nanocrystalline Materials: Preparation, Properties and Applications*, Springer, 2001.

58. F.E. FUJITA [ed.], *Physics of New Materials*, Springer Series in Materials Science, 1998.

59. D.L. BISH and J.E. POST, Modern powder diffraction, *Reviews in Mineralogy*, Vol.20, Mineralogical Society of America, Washington DC 1989.

60. R.A. YOUNG [ed.], *The Rietveld Method*, International Union of Crystallography, Oxford University Press, 1993.

61. H.P. KLUG and L.E. ALEXANDER, *X-Ray Diffraction Procedures*, John Wiley & Sons, 1954.

62. R. SHUTTLEWORTH The surface tension of solids, *Proceedings of the Physical Society (London)*, Vol.A63, pp.444-457, 1950.

63. C.W. MAYS, J.S. VERMAAK, and D. KUHLMANN-WILSDORF, On surface stress and surface tension, II: Determination of the surface stress of gold, *Surface Science*, Vol.12, pp.134-140, 1968.

64. J.S. VERMAAK, C.W. MAYS, and D. KUHLMANN-WILSDORF, On surface stress and surface tension, I: Theoretical considerations, *Surface Science*, Vol.12, pp.128-133, 1968.

65. R.C. CAMMARATA, Surface and interface stress effects on interfacial and nanostructured materials, *Materials Science and Engineering*, Vol.A237, pp.180-184, 1997.

66. J.-P. BOREL and A. CHATELAIN, Surface stress and surface tension: equilibrium and pressure in small particles, *Surface Science*, Vol.156, pp.572-579, 1985.

67. R.C. CAMMARATA, Thermodynamic model for surface reconstruction based on surface stress effects, *Surface Science Letters*, Vol.273, pp.L399-L402, 1992.

68. J. WEISSMUELLER and J.W. CAHN, Mean stresses in microstructures due to interface stresses: a generalization of a capillary equation for solids, *Acta materialia*, Vol.45, pp.1899-1906, 1997.

69. H. KUNG and T. FOECKE, Mechanical behavior of nanostructured materials, *MRS Bulletin*, pp.14-15, February 1999.

70. C.C. KOCH, D.G. MORRIS, K. LU and A. INOUE, Ductility of nanostructured materials, *MRS Bulletin*, pp.54-58, February 1999.

71. T.G. NIEH and J. WADSWORTH, Hall-Petch relation in nanocrystalline solids, *Scripta Metallurgica et Materialia*, Vol.25, pp.955-958, 1991.

72. J.Z. JIANG, J. STAUN-OLSEN, L. GERWARD and S. MØRUP, Enhanced bulk modulus and reduced transition pressure in γ-Fe_2O_3 nanocrystals, *Europhys. Lett.*, Vol.44, pp.620-626, 1998.

73. H. HAHN and R. AVERBACK, High temperature mechanical properties of nanostructured ceramics, *Nanostructured Materials*, Vol.1, pp.95-100, 1992.

74. R.S. AVERBACK, Sintering and deformation of nano-grained materials, *Zeitschrift für Physik*, Vol.D26, pp.84-88, 1993.

75. S. TSUREKAWA, K. ISHIKAWA, Z.-Q. LI, Y. KAWAZOE and A. KASUYA, Origin of anomalous lattice expansion in oxide nanoparticles, *Phys. Rev. Letters*, Vol.85, pp.3440-3443, 2000.

76. PH. BUFFAT and J.-P. BOREL, Size effect on the melting temperature of gold particles, *Physical Review*, Vol.A13, pp.2287-2298, 1976.

77. P.R. COUCHMAN and W.A. JESSER, Thermodynamic theory of size dependence of melting temperature in metals, *Nature*, Vol.269, pp.481-483, 1977.

78. A.P. ALIVISATOS, Semiconductor nanocrystals, *MRS Bulletin*, August, pp.23-32, 1995, (quantum confinement).

79. J. HARADA and K. OHSHIMA, X-ray diffraction study of fine gold particles prepared by gas evaporation technique, *Surface Science*, Vol.106, pp.51-57, 1981.

80. C. SOLLIARD and M. FLUELI, Surface stresses and size effect on the lattice parameter in small particles of gold and platinum, *Surface Science*, Vol.156, pp.487-494, 1985.

81. J. WOLTERSDORF, A.S. NEPIJKO and E. PIPPEL, Dependence of lattice parameters of small particles on the size of the nuclei, *Surface Science*, Vol.106, pp.64-69, 1981.

82. A.M. STONEHAM, Measurement of surface tension by lattice parameter changes: theory for facetted microcrystals, *Journal of Physics C: Solid State Physics*, Vol.10, pp.1175-1179, 1977.

83. F.W.C. BOSWELL, Precise determination of lattice constants by electron diffraction and variations in the lattice constants of very small crystallites, *Proceedings of the Physical Society (London)*, Vol.A64, pp.465-476, 1951.

84. S.B. QADRI, J. YANG, B.R. RATNA, E.F. SKELTON, and J.Z. HU, Pressure induced structural transition in nanometer size particles of PbS, *Applied Physics Letters*, Vol.69, pp.2205-2207, 1996.

85. M. R. SILVESTRI and J. SCHROEDER, The size dependence of the high-pressure phase stability of II-VI semiconductor nanocrystals, *Journal of Physics: Condensed Matter*, Vol.7, pp.8519-8527, 1995.

86. S.H. TOLBERT and A.P. ALIVISATOS, Size dependence of the solid-solid phase transition in CdSe nanocrystals, *Journal of Physics*, Vol.D26, pp.56-58, 1993.

87. S.H. TOLBERT, S.H. and A.P. ALIVISATOS, The wurtzite to rock salt structural transformation in CdSe nanocrystals under high pressure, *Journal of Chemical Physics*, Vol.102, pp.4642-4656, 1995.

88. J.N. WICKHAM, A.B. HERHOLD and A.P. ALIVISATOS, Shape change as an indicator of mechanism in the high-pressure structural transformations of CdSe nanocrystals, *Phys. Rev. Letters*, Vol.84, pp.923-926, 2000.

89. B. BONDARS, S. GIERLOTKA, and B. PAŁOSZ, Program for simulation of diffraction patterns of small particles, *Materials Science Forum*, Vol.133-136, pp.301-306, 1993.

90. R. PIELASZEK, S. GIERLOTKA, S. STEL'MAKH, E. GRZANKA, and B. PAŁOSZ, X-Ray characterization of nanostructured materials, *Proceedings of the 4th High Pressure School on Chemistry, Biology, Materials Science and Techniques*, Warsaw, June 22-25, 2001, Defect and Diffusion Forum - 2002 [in press].

91. T. UNGAR, H. MUGHRABI, D. ROENNPAGEL and M. WILKENS, X-ray line broadening study of the dislocation cell structure in deformed [001]-oriented copper single crystals, *Acta Metallurgica*, Vol.32, pp.333-342, 1984.

92. D.G. KEIL, H.F. CALCOTE and R.J. GILL, Flame synthesis of high purity nanosized crystalline silicon carbide powders, *MRS Symp. Proceedings*, Vol.410, pp.167-172, 1996.

93. J.F. JANIK and J.R. WELLS, Gallium imide $\{Ga(NH)_{3/2}\}_n$ a new polymeric precursor to gallium nitride powders, *Chem. Mater.*, Vol.8, pp.2708-2713, 1996.